ISTANBUL TECHNICAL UNIVERSITY ★ GRADUATE SCHOOL OF SCIENCE
ENGINEERING AND TECHNOLOGY

# FABRICATION AND CHARACTERIZATION OF ULTRA HIGH PERFORMANCE CNTS/PEI NANOCOMPOSITE FILAMENTS FOR ADDITIVE MANUFACTURING

**M.Sc. THESIS**

**Özge KAYNAN**

**Department of Textile Engineering**

**Textile Engineering Program**

**JUNE 2018**

ISTANBUL TECHNICAL UNIVERSITY ★ GRADUATE SCHOOL OF SCIENCE
ENGINEERING AND TECHNOLOGY

# FABRICATION AND CHARACTERIZATION OF ULTRA HIGH PERFORMANCE CNTS/PEI NANOCOMPOSITE FILAMENTS FOR ADDITIVE MANUFACTURING

**M.Sc. THESIS**

**Özge KAYNAN**
**(503161829)**

**Department of Textile Engineering**

**Textile Engineering Program**

**Thesis Advisor: Asst. Prof. Elif Özden Yenigün**

**JUNE 2018**

İSTANBUL TEKNİK ÜNİVERSİTESİ ★ FEN BİLİMLERİ ENSTİTÜSÜ

# EKLEMELI İMALAT İÇİN ULTRA YÜKSEK PERFORMANSLI İLETKEN NANOKOMPOZİT FİLAMANLARIN ÜRETİMİ VE KARAKTERİZASYONU

**YÜKSEK LİSANS TEZİ**

**Özge KAYNAN**
**(503161829)**

**Tekstil Mühendisliği Anabilim Dalı**

**Tekstil Mühendisliği Programı**

**Tez Danışmanı: Dr. Öğr. Üyesi Elif Özden Yenigün**

**HAZİRAN 2018**

Özge KAYNAN, a M.Sc. student of ITU Graduate School of Science Engineering and Technology 503161829 successfully defended the thesis entitled “FABRICATION AND CHARACTERIZATION OF ULTRA HIGH PERFORMANCE CNTS/PEI NANOCOMPOSITE FILAMENTS FOR ADDITIVE MANUFACTURING”, which she preparedafter fulfilling the requirements specified in the associated legislations, before the jurywhose signatures are below.

| | | |
|---|---|---|
| **Thesis Advisor :** | **Asst. Prof. Elif Özden Yenigün**<br>Istanbul Technical University | .............................. |
| **Jury Members :** | **Prof. Hale Canbaz Karakaş**<br>Istanbul Technical University | .............................. |
| | **Assoc. Prof. Fevzi Çakmak Cebeci**<br>Sabancı University | .............................. |

**Date of Submission :** **04 May 2018**
**Date of Defense :** **08 June 2018**

*To my lovely mother,*

**FOREWORD**

First and foremost, I am honestly thankful to my advisor, Dr. Elif Özden Yenigün for her guidance, support and her advising. I have learned a lot from her since the beginning of my undergraduate studies. Under her advising, I worked various research projects and I gained remarkable research experience. Also, I would like to gratitude towards my other mentor Dr. Hülya Cebeci. I am appreciative for her support, advises, and constructive criticisms particularly developed my research and presentation skills. My both supervisors became a role model for me that they constituted as successful researchers and good people. I am deeply thankful to them.

I am also thankful to Boeing Global Technology Co. entitled project "Ultra High Performance Conductive Thermoplastic Cellular Nanocomposites by 3D Printing" for equipment supports, TUBITAK Project Numbered (116M427)"Production of Vertically Aligned Carbon Nanotube Reinforced Nanoprepregs and Their Use in Thermoplastic Composites for Reinforcing Interface" for scholarship support, and ITU BAP Project Numbered (2017-40710) for material supports, provided during my graduate studies.

I would like to give special thanks goes to my labmate PhD Candidate Alptekin Yıldız for his supports and helps. Also, special thanks to Beyza Bozali, Fırat Turgut and İdris Gürkan for their huge help for mechanical testing and lab processing supports for this thesis and also for the previous works. Furthermore, I am grateful to Dr. Gülcan Çorapcıoğlu and MSc student Barış Emre Kıral from Sabanci University for their characterization supports.

I am deeply thankful to my beloved one, Mehmet Uğur Akçal, for his support, patience and being with me anytime I need. I can't thank him enough for encouraging me.

Last but not least that I am greatly thankful to my mother, Özlem Kaynan, my father, Erol Kaynan, and my brother, İ. Kubilay Kaynan for all their endless support, encouragement and motivation. I will be always grateful for them for everything they have done.

June 2018

Özge KAYNAN
(Textile Engineer)

**TABLE OF CONTENTS**

**Page**

## ABBREVIATIONS

**AM** : Additive Manufacturing
**3D** : Three-Dimensional
**CAD** : Computer-Aided Design
**STL** : Surface Tessellation Language
**g-code** : Geometric Code
**FDM** : Fused Deposition Modelling
**SLS** : Selective Laser Sintering
**SLA** : Stereolithography
**UV** : Ultraviolet
**ABS** : Acrylonityle Butadiene Styrene
**PLA** : Polylactic Acid
**PP** : Polypropylene
**PE** : Polyethylene
**PC** : Polycarbonate
**PET** : Polyethylene Terephthalate
**PSU** : Polysulfone
**PAEK** : Polacryloetherketone
**PEK** : Polyetherketone
**PPS** : Phenylene Sulphone
**PA** : Polyamide
**PBT** : Polybutylene Terephthalate
**LDPE** : Low Density Polyethylene
**HDPE** : High Density Polyethylene
**NMP** : N-Methyl-2-Pyrrolidone
**DMF** : Dimethylformamide
**DMAc** : Dimethylacetamide
**PEEK** : Polyetheretherketone
**s-PEEK** : Sulphonated-Polyetheretherketone
**PEI** : Polyetherimide
**CNT** : Carbon Nanotubes
**MWCNT** : Multi Walled Carbon Nanotubes
**SWCNT** : Single Walled Carbon Nanotubes
**TNPP** : Trisnonylphenylphosphite
**DSC** : Differential Scanning Calorimeter
**r-GO** : Reduced Graphene Oxide
**TGA** : Thermogravimetric Analysis
**SEM** : Scanning Electron Microscopy
**FESEM** : Field Emission Scanning Electron Microscopy
**TEM** : Transmission Electron Microscopy
**Tg** : Glass Transition Temperature

## SYMBOLS

| | |
|---|---|
| **L** | : Length |
| **D** | : Diameter |
| **d** | : Density |
| **E** | : Modulus of Elasticity |
| $\sigma_{\mathbf{m}}$ | : Tensile Strength |
| $\varepsilon$ | : Elongation |
| $\delta_{\mathbf{d}}$ | : Hansen Solubility Parameter of Dispersion Forces |
| $\delta_{\mathbf{p}}$ | : Hansen Solubility Parameter of Polarity |
| $\delta_{\mathbf{H}}$ | : Hansen Solubility Parameter of Hydrogen Bond Interaction |
| **S** | : Resolved mallest Distance of TEM |
| $\lambda$ | : Wavelength |
| $\beta$ | : Semi-Angle of Magnifying Lens Correlation |
| **R** | : Resistance |
| $\rho$ | : Electrical Resistivity |
| **I** | : Current |
| **V** | : Voltage |
| **A** | : Area |
| **F** | : Correlation Factor |
| $\mathbf{F_1}$ | : Geometric Correlation factor of Finite Thickness Sample |
| $\mathbf{F_2}$ | : Probe Alignment in Edge of Sample |
| **l** | : Distance of Current Probes |
| **s** | : Specimen Thickness |
| $\phi_{\mathbf{c}}$ | : Minimum Amount of Conductive Filler |

## LIST OF TABLES

## LIST OF FIGURES

**Page**

## FABRICATION AND CHARACTERIZATION OF ULTRA HIGH PERFORMANCE CNTS/PEI NANOCOMPOSITE FILAMENTS FOR ADDITIVE MANUFACTURING


### SUMMARY

Additive manufacturing (AM) or three-dimensional (3D) printing by another name produces a diverse range of geometrical shapes by layer by layer deposition while eliminating post-processes such as cutting and trimming. Fused deposition method (FDM) has been most widely used 3D printing technology that works with the principle of layer by layer deposition of guiding melted thermoplastic filaments. So far, due to their low cost and easy processability acrylonitrile butadiene styrene (ABS), polylactic acid (PLA) and polyamide (PA) have been most used thermoplastic polymers. However, they are not strong and durable enough to tolerate high loads particularly in structural components. Besides, due to the intrinsically restricted mechanical response of these printed polymer structures, there is significant demand to fabricate high performance structures by using 3D printers. Thus, high performance thermoplastic materials such as polyetherimide (PEI) and polyether ether ketone (PEEK) have been found promising as competitors to strong and conductive but relatively dense metals and metal alloys in aerospace applications. Even though, there are still processing challenges such as high melting temperatures and the need of good control on ambient temperature, 3D printing technique offers many advantages in the fabrication of structural polymer based components, including high precision, cost effectiveness and customized complex 3D geometries. Another asset to utilize strong but light weight polymer filaments in 3D printers is their ability to tune their micro structures by incorporating nanomaterials. Among many nanomaterials, carbon nanotubes (CNTs) have been a substantial area of research over last two decades due to nanotubes' high aspect ratio, low mass density and superior electrical, mechanical and thermal properties. Novel advanced materials produced from CNTs blended with amorphous high performance PEI polymers, provide new capabilities and new skills in aerospace applications.

Not only engineered materials but also the use of 3D printing technology facilitates chemically and thermally resistant and conductive prototype production with complex geometries. More importantly, 3D printed objects fabricated by using conductive filler reinforced filaments have ability to conduct electrons. All these efforts on nanocomposite filaments addresses the possibilities to replace metals and metal alloys. This thesis attempts to explore CNTs reinforced PEI nanocomposite conductive filament fabrication by melt processing and their later use in AM process.

First, customized twin-screw and single-screw extruders were designed to process high performance polymers including PEI and PEEK thermoplastics. Then, neat PEI filaments, and 5 and 7 wt % CNTs/PEI nanocomposite filaments were fabricated by using consecutive single and twin-screw extrusion processes. Prior to single-screw extrusion, CNTs and PEI granules were directly fed through twin-screw extruder to produce CNTs/PEI blended pellets. To ensure homogeneous CNTs dispersion

in PEI matrix that dictates the electrical conductivity and mechanical performance of nanocomposite, twin-screw extrusion was repeated for five times and then nanocomposite strands were granulized to be later fed into the single extruder to produce CNTs/PEI nanocomposite filaments. CNTs reinforced nanocomposite filaments were fabricated with diameter of 1.70 mm, which was specifically aimed for additive manufacturing.

Thermal characterization of both neat PEI and CNTs/PEI samples was performed by Differential Scanning Calorimeter (DSC) which pointed out that the introduction of CNTs did not change thermal transition of PEI. Thermogravimetric analysis (TGA) revealed that CNTs caused slight shift in decomposition temperature compared to neat PEI. Morphological studies of both scanning electron microscopy (SEM) and transmission electron microscopy (TEM) revealed that CNTs were homogeneously dispersed and distributed in PEI matrix. TEM micrographs clearly pointed out that CNTs were also oriented along extrusion direction without having any curly conformation or agglomerated CNTs clusters due to flow induced orientation. This effect positively contributed both to tensile properties and, conductivity by reducing percolation threshold of CNTs/PEI filaments. Volume conductivity measurements by four point probe method showed that CNTs presence in the PEI matrix significantly increased the conductivity. For 7 wt % CNTs/PEI filaments, surface conductivity was achieved up to $2.57 \times 10^{-1}$ S/cm. Percolation threshold of CNTs/PEI nanocomposite system was estimated between 0.1 and 0.25 wt %, which was remarkably lower than reference studies in literature. Moreover, specific stiffness showed gradual increase up to 20 % with CNTs addition where specific tensile strength of nanocomposite filaments with 7 wt % CNTs reinforced improved about 10 % compared to neat PEI specimen.

Overall, this thesis traces the effect of CNTs on electrical and mechanical properties of CNTs/PEI 3D printer filaments and also highlights the process and material requirements to work with structural polymers in melt processes.

**EKLEMELI İMALAT İÇİN**
**ULTRA YÜKSEK PERFORMANSLI İLETKEN**
**NANOKOMPOZİT FİLAMANLARIN ÜRETİMİ VE KARAKTERİZASYONU**

## ÖZET

Eklemeli imalat diğer bir isimle üç boyutlu (3D) yazıcılar kesme ve düzenleme gibi işlem sonrası ekstra çalışmaları ortadan kaldırırken, katman üzerine katman biriktirmesi yöntemi ile çok çeşitli geometrik şekiller üretir. Eriyik yığma modelleme 3D yazıcı teknolojinin en çok kullanılan yöntemlerinden biridir. Bu metot termoplastik filamanı hammadesi olarak kullanır ve eriğik termoplastiği katman katman biriktirme prensibine dayanarak çalışır. Şimdiye kadar eriğik yığma metodu ile sahip oldukları uygun fiyat ve kolay üretilebilirlik sebebiyle Akrilonitril Bütadiyen Stiren (ABS), polilaktik asit (PLA), poliamid (PA) en çok kullanılan polimerlerdir. Fakat bu polimerler yeterince sağlam ve dayanıklı olmadıkları için yapısal parça olarak yük taşımaya uygun değildirler. Ayrıca, bu polimerler kullanılarak üretilen yapılar da mekanik olarak kısıtlı olmaktadır. Bu sebeple yüksek performans polimerleri kullanıralarak üretilen 3D yapılara ciddi bir şekilde ihtiyaç duyulmaktadır. Dolayısıyla, polieter imid (PEİ) ve polietereterketon (PEEK) gibi yüksek performans termoplastik malzemeleri güçlü iletken fakat yoğukça fazla metal ve metal alaşımlarının havacılık alınındaki kullanımda yerlerini alması için gelecek vaadeden polimerler olarak görülmektedir. Bu polimerlerin yüksek işlem sıcaklığı ve iyi çevre koşul gerekçeleri gibi zorlukları olmasına rağmen 3D baskı polimer bazlı 3D yapısal parçaların üretilmesinde yüksek hassasiyet, maliyet etkinliği ve özelleştirilmiş karmaşık 3D geometrilerde parça üretim imkanını içeren avantajlar sağlamaktadır. Başka bir kazanç ise polimer filamanlara nanomalzemelerin katılıp mikro yapılarını ayarlanmasıyla 3D yazıcılarda güçlü ama hafif polimer filamanları kullanma imkanı sağlanmaktadır. Birçok nanomalzeme arasında sahip oldukları yüksek en boy oranı, düşük kütle yoğuklukları ve üstün elektrik, mekanik ve termal özellikleri sayesinde karbon nanotüpler (KNTler) geçtiğimiz yıllarda araştırma odağı olmuştur. KNTlerin amorf yüksek performans PEİ polimerleri ile karıştırılması ile yeni kapasiteleri ve yenetekleri olan ve havacılık alanında uygulanabilir özgün geliştirilmiş malzemeler üretilmesi sağlamaktadır.

Mühendislik malzemeleri ile 3D yazıcı teknolojisinin birleşimi kimyasal ve termal kararlı ve kompleks geometride iletken prototiplerin oluşumuna imkan sağlamaktadır. Daha da önemlisi, iletken katkı malzemeleriyle katkılandırılmış filamanlardan üretilen 3D objeler elektronları iletebilme özelliğine sahiptirler. Nanokompozit filamanlar üzerinde yapılan tüm bu yenilikçi yaklaşımlar özellikle havacılık gibi yüksek performans gerektiren alanlarda metal ve metal alaşımı yerine kullanımına olanak sağlaması amacıyla yapılmaktadır. Düşük yoğunluklu olan polimerlerin metallerin yerine geçmesiyle örneğin uçaklarda ağırlık azalması ve dolayısıyla harcanan yakıtın azalmasına olanak sağlamaktadır. Bu tez 3D yazıcılarda kullanılmak üzere KNT katkılı PEİ nanocompozit filamanların eriyik işlemi ile üretilmesini araştırmaktadır.

İlk olarak isteğe göre uyarlanmış çift burgu ve tek burgu ekstruderler PEİ ve PEEK gibi termoplastikleri içeren yüksek performans polimerlerini işleme amacıyla tasarlanmıştır. Sonrasında, saf ve kütlece % 5 ve 7 KNT katkılı filamanlar çift ve tek burgu ekstruderleri kullanılarak üretilmiştir. Saf PEİ filamanı üretmek için kimyasal veya akışkanlandırıcı kullanılmadan sadece tek burgu ektruderi kullanılarak üretilmiştir. KNT katkılı polimerler ise hem çift hem de tek burgu vidalı ekstruderler kullanılarak hiç bir katkı maddesi kullanılmadan üretilmiştir. Tek burgu öncesinde, KNTler yan beslemeden ve PEİ granülleri ana beslemeden olmak üzere çift burgu ektrudere beslenmiş ve nanokompozitlerin granülatör aracılığıla kesilmesiyle KNT/PEİ nanokompozit granülleri elde edilmiştir. Kompozitin hem elektrik iletkenliğini hem de mekanik performansını etkileyeceği için KNTlerin PEİ içerisinde homojen olarak karışmasını sağlamak amacıyla çift burgu karışımı beş kere tekrarlandıktan sonra nanokompozitler granülatör ile kesilerek tek burgu ekstruderde işlem için hazırlanmıştır. 3D yazıcıya uygun olacak şekilde, KNT/PEİ granülleri sonrasında tek burgu ekstrüderine beslenerek 1.70 mm filamanlar üretilmiştir.

Hem saf PEİ hem de KNT katkılı PEİ için diferansiyel taramalı kalorimetre (DSC) ve termogravimetrik analiz (TGA) aracılığı ile termal karakterizasyon yapılmıştır. DSC sonuçlarına bakıldığında KNT katkısının PEİ'nin termal geçişini değiştirmediği görülmüştür. Bunun sebebinin eriyik işlem sırasında uygulanan yüksek kayma stresinden dolayı KNTlerin boylarında oluşan kısalma olduğu düşünülmektedir. TGA sonuçlarında KNT etkisinin PEİ'nin ayrışma sıcaklığında kaymaya sebep olduğu görülmektedir. 3D yazıcı ektrüzyonu için de önemli olarak, KNTlerin PEİ'nin termal geçişlerini ve termal bozulmasına önemli bir etkisi olmadıgı rapor edilmiştir. Taramalı elektron mikroskobu (SEM) ve geçirimli elektron mikroskobu (TEM) aracılığı ile morfolojik analiz yapılmıştır. SEM görüntülerinde KNTlerin PEİ matrisi içinde homojen olarak dağıldığı görülmektedir. Odaklanmış yükün demetli (FIB) mikroskobu ile 100 nm kalınlığında hazırlanan aüırlıkça % 0.1 ve 7 KNT/PEİ filamanlarına TEM analizi yapılmıştır. TEM görüntülerinde açıkça görüldüğü üzere KNTler PEİ matrisinde aglomere olmamasının yanı sıre hem homojen olarak dağılmış hem de dağıtılmiştir. Fakat aynı zamanda KNTlerin boylarında ciddi bir düşüş gözlemlenmiştir. Ekstrüzyon işlemi sonrası KNTlerin boyları 305 nm aralığında olduğu saptanıştır. Bu düşüşün temel sebebinin tekrarlı şekilde uygulanan çift burgu ekstrüzyonu olduğu düşünülmektedir. Ayrıca TEM görüntülerinden açıkça görüldüğü üzere KNTler ekstrüzyon ekseninde yönlenmiştir. Bu durum nanokompozit filamanların çekme mukavemetine ve elektrik iletkenlik özelliklerine sızıntı eşiğini düşürerek pozitif katkı yaptığı düşünülmektedir. KNT katkılı PEİ filamanlarının elektrik iletkenliği KNT miktarı arttıkça artış göstermiştir. Saf PEİ'nin yüzey iletkenliği $10^{-15}$ S/cm iken ağırlıkça % 7 KNT/PEİ filamanının yüzey iletkenliği $2.57x10^{-1}$ S/cm olarak saptanmıştır. KNT/PEİ nanokompozit sisteminin sızıntı eşiği kütlece % 0.1 ile 0.25 arasında olduğu sonucuna varılmıştır. Bu sonuç diğer polimer sistemleriyle karşılaştırıldığında oldukça düşüktür. Bunun sebebi hem KNTlerin homojen olarak dağılması hem de PEİ matriksinin sahip olduğu yüksek viscozite olduğu düşünülmektedir. Ayrıca, KNT eklenmesi hem özgül esnemezlik hem de özgül mukavemette atrtış gösterdiği görülmektedir. Kütlece % 7 KNT katkısı saf PEİ filamana göre özgül esnemezliği % 20 ve özgül mukavemeti % 10 arttırdığı gözlemlenmiştir.

Sonuç olarak bu tezde KNT eklemenin PEİ filamanı üzerinde elektrik ve mekanik özellikleri üzerine etkisi incelenmiştir. Ek olarak, 3D yazıcıda üretilebilir yapısal polimerler için işlem ve malzeme gerekçeleri üzerinde durulmuştur. KNT katkisinin 3D yazıcılar için tasarlanan filamanda hem elektrik iletkenlik hem de mekanik performans olarak katkı sağladığı sonucuna varılmıştır. Morfolojik analizlerle gözlemlenen homojen KNT dağılımının hem elektriksel hem de mekanik özelliklere pozitif katkıda bulunduğu düşünülmektedir.

# 1. INTRODUCTION

## 1.1 Literature Review

### 1.1.1 Additive manufacturing for aerospace applications

Three-dimensional (3D) printing, also widely known as additive manufacturing (AM), is a material extrusion technique to fabricate the 3D object from 3D model data, generally layer upon layer. The process begins with creating a 3D model by either acquired image processing or objects designed in computer-aided design (CAD) software. The 3D model converted into Surface Tessellation Language (STL) file. SLS is then transferred by slicing software converting to two-dimensional layers as a geometric code file (g-code) the 3D model through the 3D printer.

3D printing technique offers many advantages over traditional manufacturing methods, some of which are providing design freedom due to the possibility of creating complex 3D geometries, building structural objects without assembly and reducing the waste and chemicals usage during the process [1]. However, the adaption of AM for particularly high performance required fields is limited due to the restricted material selection. Available materials have potential to be processed by AM are such as metals [2], ceramics [3], and dominantly polymers include both thermosets and thermoplastics. Thermoset polymers such as epoxy resins could be processed in AM with the aid of thermal or ultraviolet (UV) supplements. To convert liquid epoxy into the solid state during 3D printing, the thermoset resin requires either thermal of UV hardening agent regarding curing type. Thus, those polymers are appropriate for UV or thermal curable 3D printing systems. Additive manufacturing of thermoplastics, on the other hand, works by layer by layer via softening and solidifying the polymer without any demand for chemical or curing agent usage due to their linear molecular chains. Commonly used thermoplastics as 3D printing feedstock are acrylonitrile butadiene styrene (ABS) [4, 5], polylactic acid (PLA) [5, 6], polyamide (PA) [7] and polycarbonate (PC) [8].

Even though 3D printed objects have potential to use in aerospace applications [9], architecture [10, 11] and medical areas [12], most of them are not sufficient enough for use as functional components rather than prototypes [13]. 3D objects fabricated by neat polymer filaments provide lack of mechanical strength and no functionality compared to multi-functional and load bearing capable parts. Thus, the multifunctional novel nanomaterial filament feedstock is required to be investigated [14] for later process in 3D printing applications. Several properties were already incorporated into FDM filaments such as electrical and thermal conductivity. However, fabrication and adoption of multifunctional FDM filament feedstock are still an issue particularly to obtain both efficient mechanical performance and electrical conductivity. Because limited material potential to process in available 3D printers restricts the possibility of tailoring the material properties. Commercially available printers such as Mark Forged, Ultimaker create 3D parts by using conventional polymers including PA and PLA. Fabrication of multifunctional 3D printed objects requires a wide range of polymer types and suitable nanofiller selection for FDM feedstock, as well as the adoption of 3D printers regarding novel functional filaments. Thus, high-performance engineering polymers attract a great interest for AM since these thermoplastics offer superior mechanical properties, and dimensional, chemical and environmental stability even at high temperature or pressure [15].

There are various AM techniques developed and well-adapted to create 3D objects, which are Fused Deposition Modelling (FDM), Selective Laser Sintering (SLS), Inkjet 3D printing, Stereolithography (SLA) and 3D plotting as shown in Figure 1.1. SLS technique contains a laser beam that scans and conducts sintering of the powder. The main disadvantage of SLS system is the high cost of the process. Inkjet 3D printing is also powder processing method similar to SLS; however, in inkjet 3D printing, the liquid binder is used to adhere the powder instead of using a laser beam. Inkjet 3D printing is a low cost, and has multi-material process capability. SLA, on the other hand, contains a UV laser that cures the photocurable resin. Epoxy and acrylate-based resins are processed by SLA method. 3D plotting is an extrusion technique uses a viscous material from a pressurized syringe. Curing could be conducted by either thermally or using UV light. The primary advantage of 3D plotting is providing material flexibility comprising solutions, pastes, and hydrogels could be used as raw material.

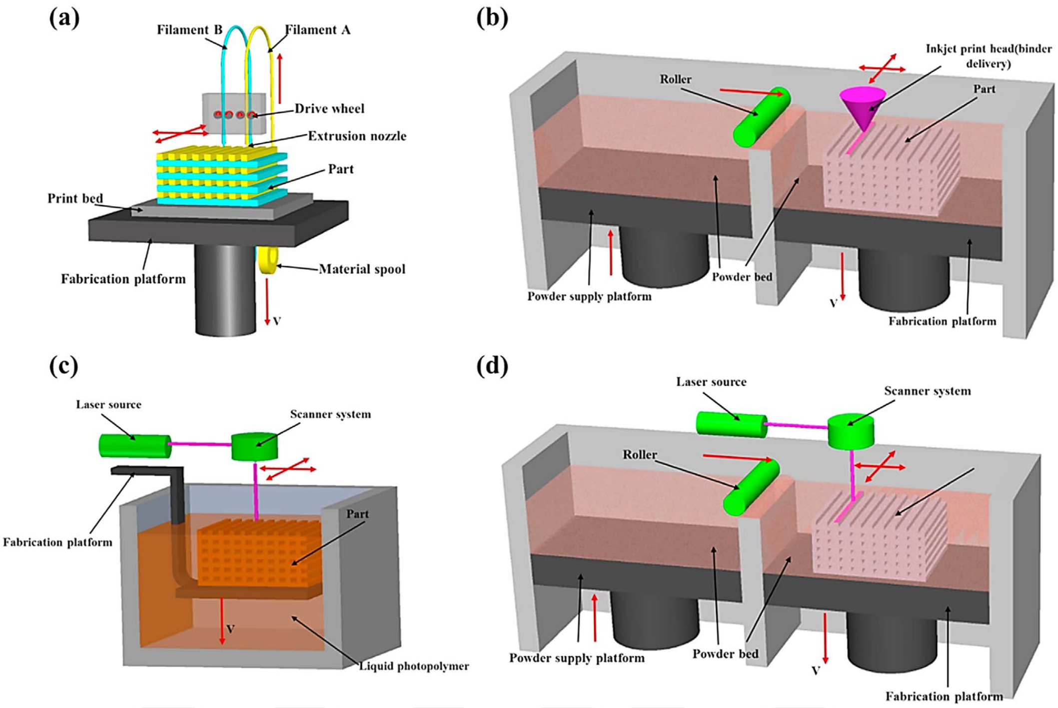


**Figure 1.1** : Various 3D printers using a) FDM, b) inkjet 3DP, c) SLA, b) SLS and e) 3D plotting setups [13].

Integration of nanotechnology into AM has potential to both to develop recent techniques and to create novel nanocomposites [1]. This approach is promising to overcome 3D printing limitations such as lack of functionality and unefficient load bearing capability, which could be accomplished by using high-performance polymers as matrix of composites. One of the widely used AM method, FDM, has potential to incorporate nanofillers into high-performance thermoplastics. This is a promising way to develop multifunctional FDM filament for later creating 3D objects. The primary drawback of FDM printer is that demand of the composite feedstock in a filament form. However, the problem is difficulty to achieve homogeneous dispersion and distribution of nanofillers in the composite filament. Also, the melt viscosity of thermoplastic matrix in the composite filament is required to be high enough to provide structural support and low enough to extrude [13].

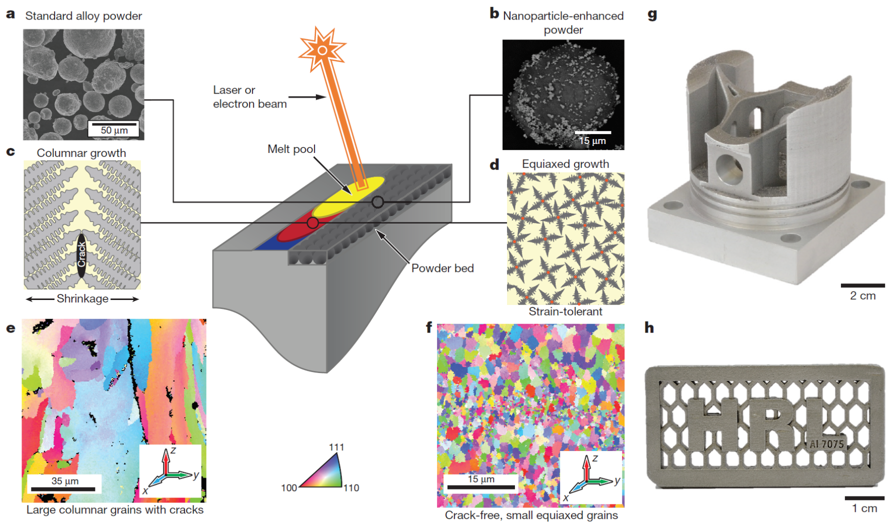


**Figure 1.2** : Metal printing for aerospace applications reported in reference study [16].

Aerospace components are usually in the form of complex geometries. Therefore, manufacturing these structural objects with traditional techniques is costly in terms of both price and time which in turn restricts the design freedom. Hence, AM is a convenient method to create components with complex geometries [13]. Since metals have higher strength and are more retardant than polymers, such components like turbine blade and engine exhaust were metal 3D printed components as reported by some researchers [17, 18]. In a recent study, Martin *et al.* [16] created aluminum alloy applicable to additive manufacturing particularly selective laser melting. The aluminum was become suitable for 3D printing by incorporating nanoparticles into nucleants that assisted to control solidification of the structures during 3D printing. Eventually, crack-free, equiaxed and fine-grained 3D printed components were obtained as it can be seen in Figure 1.2. Tensile strength results of this study revealed that additive free aluminum component showed almost no strength due to the high number of cracks. Moreover, $AlSi_{10}Mg$ demonstrated high ductility and high strength compared to neat 3D printed aluminum. Furthermore, 3D printed samples with incorporated $Al_3Zr$ nucleants pointed out 80% improvement in tensile strength regarding $AlSi_{10}Mg$ sample owing to the lack of cracks and extremely small grain sizes around $10\mu m$.

Polymers have several significant advantages for aerospace applications compared to metals due to their low specific densities and low weight, which led to fuel efficiency.

Invernizzi [19] *et al.* reported glass fiber and carbon fiber reinforced 3D printed airfoil and propeller by UV assisted 3D printing technique as seen in Figure 1.3. Efficient mechanical properties were obtained in those 3D printed components due to superior interlayer bonding between the layers.

3D printed polymer composites that retain at relatively high temperatures are promising for aerospace applications. Chopped carbon fiber reinforced PEI filaments were fabricated for FDM applications and inlet guide vane produced by 3D printing, which can withstand up to 200°C [20]. Moreover, Impossible Objects company [21] manufactured carbon fiber/ polyetheretherketone (PEEK) composites for aerospace applications such as particularly airfoil, rotor support arm and air intake.

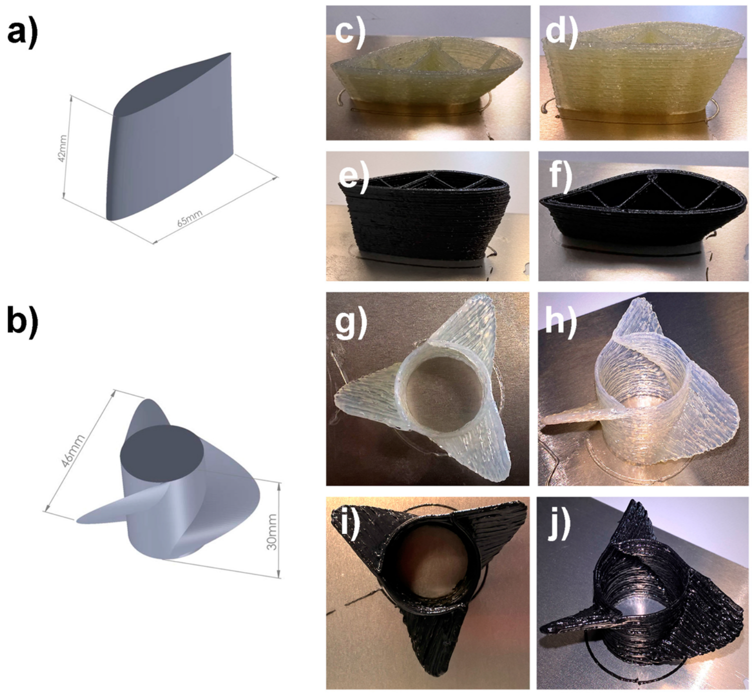


**Figure 1.3** : 3D printed airfoil and propeller by UV assisted 3D printing [19].

### 1.1.2 High performance thermoplastic polymers and their potential use in additive manufacturing

Thermoplastic polymers consist of simple long chains which are chemically independent molecules. As these plastics can be heated, softened/melted, and they could be shaped or welded. Then, the thermoplastics are solidified and shaped by cooling with air or water. These polymers can be heated repeatedly without any damage, thus they can be re-processable and recyclable. These plastics' process cycle is short compared to thermosets since no chemical reaction of cross-linking takes place during formation. Thermoplastic polymers usually are combined with fillers, which phenomena known as composites, to improve several properties of composites such as electrical and mechanical properties, thermal stability. Reinforcement could be performed in several ways including short, long or continuous fibers. Thermoplastic polymers can be basicly divided into two categories, which are the commodity and high-performance polymers. Commodity polymers such as PLA and polypropylene (PP) have a low melting point, low cost, easy processability but inefficient mechanical, thermal and electrical properties. In contrast, high-performance polymers have potential to maintain effective mechanical performance and to resist harsh ambient conditions such as high temperature, high pressure, and corrosive atmospheres. The reason of which efficient strength originated from the high bonding energy in their structures due to lots of C=C and aromatic bonds [15].

Throughout thermoplastics, polyacrylketone family such as PEEK, polyacrylether-ketone (PAEK) and polyetherketones (PEK) as demonstrated in Figure 1.4, poly-imides like polyetherimide (PEI), polysulfone (PSU) have potential to use in high-performance demanded fields. The polyacrylketone family offers high mechanical properties compared to commodity polymers, chemical and environmental resistance, relatively high service temperature where above 250°C, rigid structure, fatigue resistivity, lack of shrinkage and moisture uptake and high energy radiation resistance. These positive features of polyacrylketones make them appropriate material for use in high-performance property demanded areas such as aerospace, automotive, medicine. Also, polyacrylketones could be processed by extrusion, injection, compression, molding [22]. Throughout polyacrylketone family, PEEK is the commonly known contains both ether and ketone bonds. The melting point of PEEK is above 300°C, and it has superior mechanical properties and thermal stability [15]. Furthermore, PEEK demonstrates chemical, flame and wear resistance. The main drawbacks of PEEK are its high cost and high process temperatures (around 360°C). Polyphenylene sulfide (PPS) is another semi-crystalline high-performance polymer contains benzene rings to bond sulfur atoms. PPS shows strong corrosion resistance particularly withstands stream, organic solvents, and bases. In addition, PPS shows high thermal and dimensional stability. Primary disadvantages of PPS are high process temperatures similar to PEEK and brittle features.

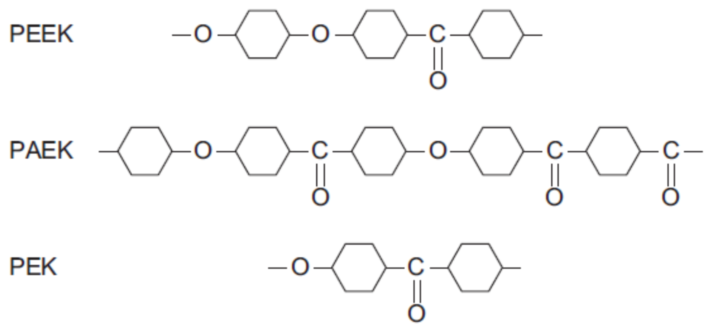


**Figure 1.4** : Polyacrylketone family of a) PEEK, b) PAEK and c) PEK [22].

Polyetherimide (PEI), also known by its trade name ULTEM, is an amorphous and high-performance thermoplastic resin that is formed by units of ether and imide linkages exhibited in Figure 1.5. Ether linkages provide flexibility, processability, and effective melting flow property, and imide units offer high-performance features and stiffness characteristics. PEI thermoplastics demonstrate high mechanical strength, inherently flame and chemical resistance, UV stability and high service temperature up to 180°C, transparent due to its amorphous structure. Also, PEI is an effective insulator even in wet and hot ambient. Due to all these advantages, PEI is a promising candidate to replace metals in lots of structures [15]. To improve its inherent properties, various fillers could be incorporated into the PEI matrix. In an old research work, glass fiber reinforced PEI revealed improvement in 40% for 30 wt % reinforcement [23]. It was reported that PEI was adhesive with glass fiber, thus mechanical performances of composites showed higher performance compared to neat samples. The application areas of PEI includes aerospace, automotive, industrial parts such as impellers, hot water reservoirs *etc.* Also, ULTEM is an efficient thermoplastic to withstand at relatively high temperatures, which has glass transition temperature (*Tg*) around 217°C. This high *Tg* of PEI provides superior retention of physical properties at high temperatures. In addition, PEI could be processed by melt extrusion, injection molding, and blow molding. The process temperature is around 350-380°C. The main drawback of PEI is inherently moisture uptake up to 0.3% [22]. Thus, before processing, the resin requires drying process in a vacuum oven at 150°C for a certain period.

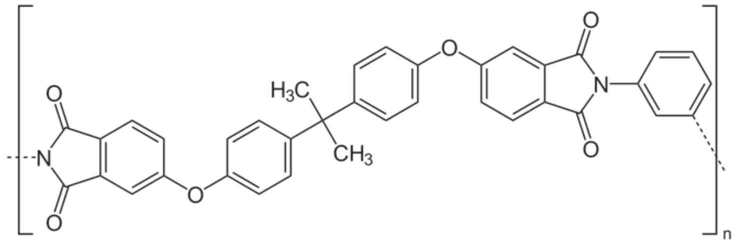

**Figure 1.5** : Chemical structure of PEI [24].

### 1.1.3 Melt processing of polymers

Extrusion process is a convenient and large-scale technique for polymeric materials. Working principle of the extruder based on that first melting the thermoplastic polymer then shaped or drawn by solidifying. Several parameters such as process temperatures, screw speed, cooling temperature *etc.* are determined considering polymer type that processed. Extruders are based on length (L) to screw diameter ratio (D), $L/D$. $L/D$ ratio is a significant feature for extrusion because throughput capacity directly depends on the ratio. The higher $L/D$, results in higher melting and mixing capacity. Screw speed is also proportional to throughput values. There are two types of melt extrusion process, which are single and twin-screw extrusions.

#### 1.1.3.1 Single-screw extrusion

Single-screw extrusion contains a sole screw that assists to apply pressure and shear to the molten polymer, which provides homogeneous melt and mixture. Barrel temperatures are set according to the polymer used and, applied heat reduces the viscosity of the polymer. Key components of single-screw extruders are drive system, feed system, screw, barrels and heater systems, head and die, and control system. The screw conveys the polymer by the assistance of applied heat and pressure through the die. Barrels' temperatures are controlled by thermocouples where inside the extruder. Air or water could be used as a cooling agent to solidify the molten polymer out of the die [25].

A single-screw, which seen in Figure 1.6, has three parts, which are feeding, transition, and metering. Feeding section conveys the polymer powder or pellet through the transition. Transition section assists to change the deep flight of unmelt polymer into melt shallow flight. In this section, melting of thermoplastic granules takes place.

Following to transition section, metering part applies the shallowest flight and high pressure to the polymer melt.

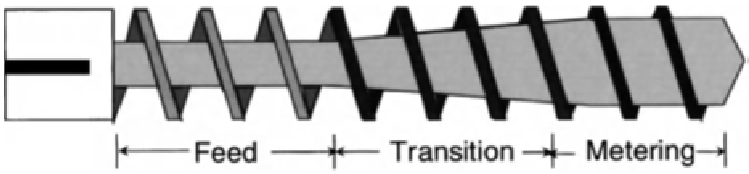


**Figure 1.6** : Single-screw sections [25].

#### 1.1.3.2 Twin-screw extrusion

Twin-screw extruders consist of two pairs of parallel screws. Different twin-screw extruders are available either co-rotating (rotating in the same direction) or counter rotating (rotating in opposite direction) with intermeshing or non-intermeshing. High-speed co-rotating twin-screw extruders are used to produce a resin with reinforcement, additives, and stabilizers whereas low-speed co-rotating and counter-rotating extruders fabricate profiles a nd p ipes. I ntermeshing i s a t erm t hat r epresents the closeness of screws of each other. Closer screws lead to creating a high shear gradient, which results in a homogeneous mixture and effective conveying. Twin-screw extruder comprises feed, screw, and barrel, die and control panel. The screw is designed as feeding, metering, conveying, mixing, pumping and venting sections, which could be modified according to polymer type. Compared to single-screw extrusion, mixing is controllable in twin-screw extrusion. Also, melt fluid is balanced by rotation of two screws and tendency of screws against closing barrels reduces [26].

Figure 1.7 demonstrates the design zones of co-rotating screws. Feeding of granules is carried out in the first zone that is cold. Zone 2 is the transition section where the polymer is melted and compressed. In zone 3, both melting and conveying of granules occur. Also, zone 3 contains right-handed kneading blocks. Following to this, zone 4 left-handed conveying kneading, which provides transporting the melt forward.

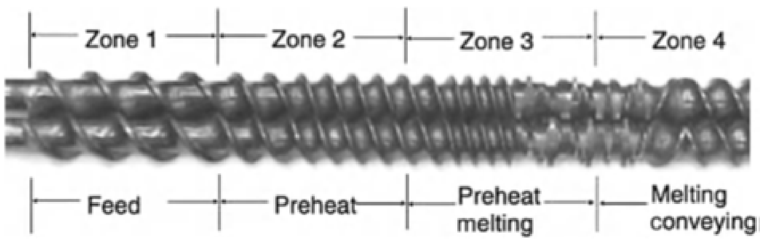


**Figure 1.7** : Twin-screw sections [25].

### 1.1.4 Carbon nanomaterials and their use in nanocomposites

Carbon is one of the most significant elements that has the ability to bond different elements in various ways. Bonding between carbon atoms is 348 $kJ/mol$, which is comparable with other carbon-based bonds such as C-O (360 $kJ/mol$) and C-H (412 $kJ/mol$). As an allotrope of carbon, diamond, which can be seen in Figure 1.8(a), has cubic and hexagonal configurations. Carbon atoms in diamond arrange in $sp^3$ bond which could be bonded to four other atoms. Graphite also another allotrope of carbon that is a stable carbon derivative at standard conditions. The structure of graphite consists of carbon hexagonal array layers as seen in Figure 1.8(b). Single carbon atoms are bonded by covalent bond whereas the hexagonal layers are fixed with w eak Van der Waals bonds. This feature provides the graphite materials superior lubricating property. Furthermore, fullerenes, which are also known as buck balls, are another form of carbon. The structure of fullerene formed by hollow cluster including 60 carbon atoms represented as C60. The average diameter of a fullerene is 1.1 nm. Figure1.8(c) shows a C60 molecule contains 12 pentagons and 20 hexagons. Fullerenes are synthesized at high pressure and high temperature by arc discharge. [27].

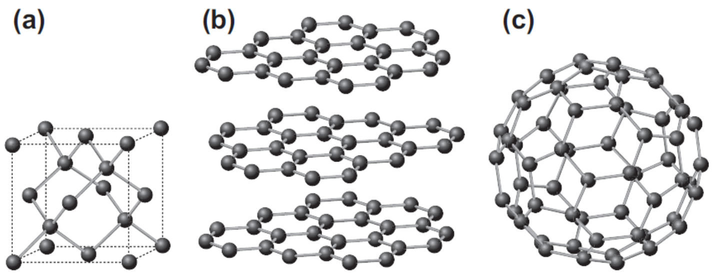


**Figure 1.8** : Carbon allotropes a) diamond, b) graphite and c) fullerene [27].

Carbon nanotubes (CNTs) are formed as a rolled a single sheet or multi sheets of graphite with a diameter of a few nanometers and a few micrometers in length. As demonstrated in Figure1.9, there are three different types of CNTs, which are single walled, double walled and multi-walled CNTs depending on the number of rolled graphite sheets in a nanotube cylinder. SWCNTs includes a single sheet of rolled graphite whereas DWCNTs consists of twofold and MWCNTs arranged by multiple graphite cylinders with a distance of 0.34$nm$ [28]. The sheets of MWCNTs were kept together by van der Waals forces.

The atomic structure of CNTs, which is commonly known as chirality or helicity is an important phenomenon, which later has a great impact on electrical conductivity of the CNTs. The chirality of the CNTs are demonstrated in Figures1.10 and 1.11. The nanotubes form in the structure of armchair (n=m), zigzag (when n or m is zero) or chiral (various n or m) considering of the nanotube appearance as seen in Figure 1.11. Van der Waals forces between the CNTs lead to aggregate the nanotubes into bundle form. The space in CNTs bundle is determined by chirality, where is 0.338 – 0.341 nm for armchair, 0.339 nm for zigzag [27]. The atomic structure of CNTs is also important since it has a great impact on electrical conductivity of nanotubes and also of resultant composites. Depending on the chiral vectors (n, m), CNTs could be metallic (conductor) or semiconductor. CNTs are conductive when m-n is multiplying of 3 [27]. Thus, armchair CNTs (n=m) are always metallic. Pure CNTs electrical conductivity is around $10^6$ – $10^7$ S/cm whereas CNTs reinforced polymer matrix composites conductivities are between 0.01 and 0.1 S/cm [29]. Specifically, MWCNTs operates as 1D conductors with high conductivity [30]. Metallic structure of MWCNTs is because of multi-cylinder structure, which leads to electronic coupling between the rolled sheets.

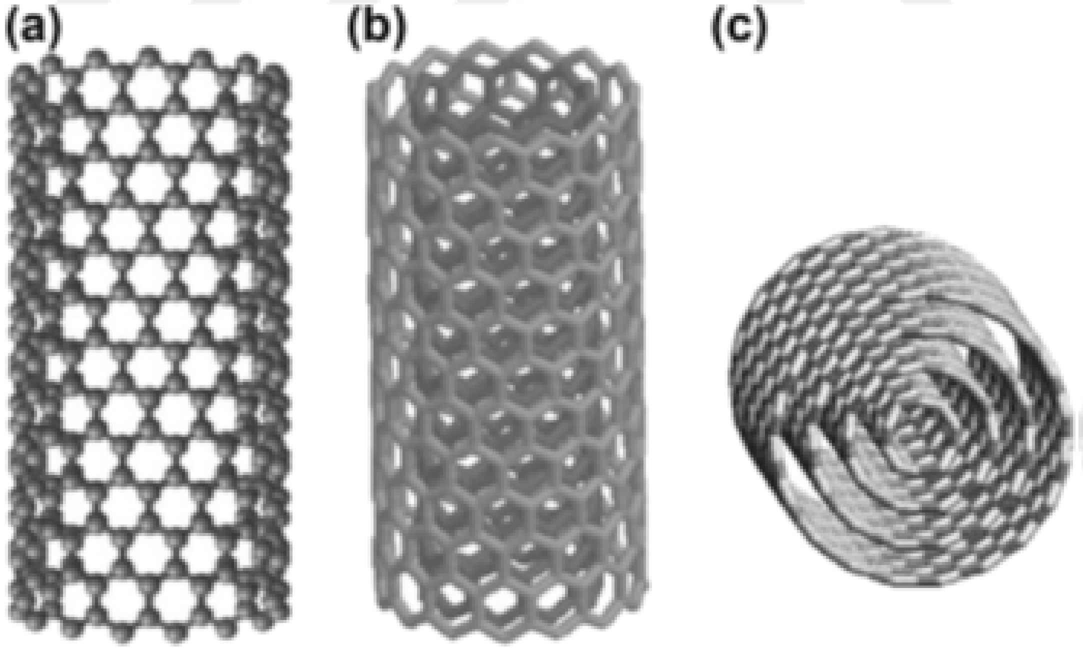


**Figure 1.9** : Schematic of a) SWCNTs, b) DWCNTs and c) MWCNTs [31].

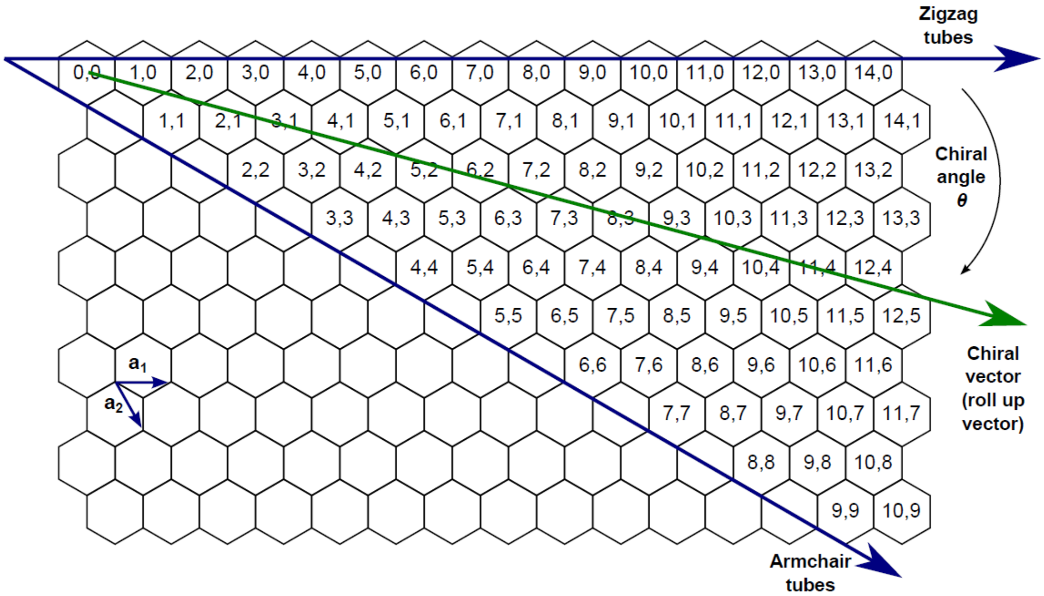


**Figure 1.10** : Chirality of CNTs [32].

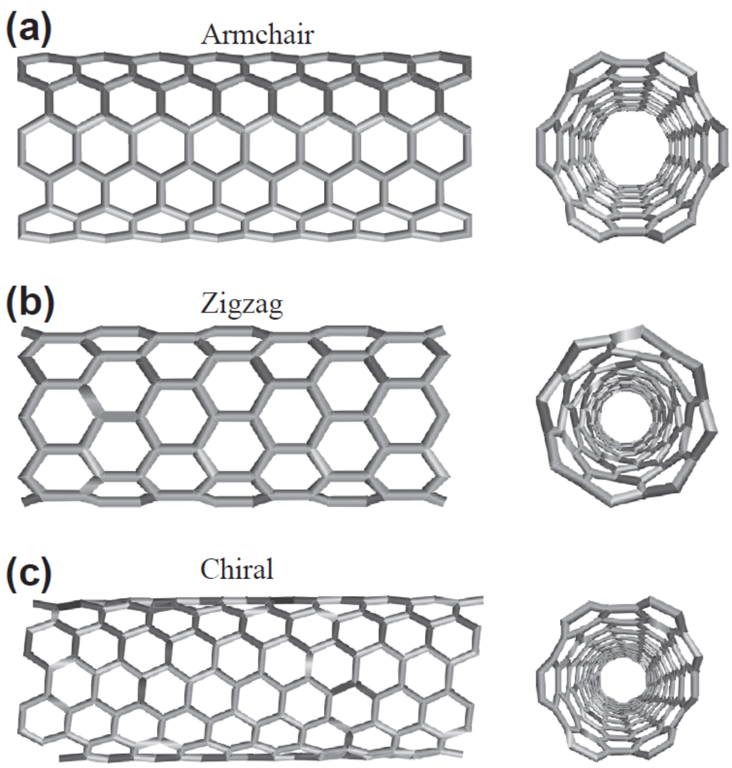


**Figure 1.11** : Chirality types of CNTs a) armchair, b) zigzag and c) chiral [32].

Both experimental and theoretical studies have reported that CNTs has the highest mechanical strength throughout the other reinforcements [33] due to carbon bonds in the structure of tubes. Specific resistance of CNTs is $48.5x10^3$ kNm/kg [34]. Providing superior strength and low density makes CNTs attractive materials for low weight and high strength required applications such as aerospace. Mechanical performances of several materials are reported in the Table 1.1, $d$, $E$, $\sigma_m$ and $\varepsilon$ represent density, Young's modulus, tensile strength, and elongation, respectively.

**Table 1.1** : Mechanical properties of several materials. [27]

| Material | $d\ (g/cm^3)$ | $E\ (GPa)$ | $\sigma_m\ (GPa)$ | $\varepsilon(\%)$ |
|---|---|---|---|---|
| SWCNTs | 1.33 | 1054 | 150 | 12 |
| MWCNTs | 2.6 | 1200 | 150 | 12 |
| Carbon fiber | 1.76 | 230 | 3.53 | 1.5 |

#### 1.1.4.1 Melt processing of structural polymers and their nanocomposites

Melt processing of thermoplastic polymers is an effective, simple and straightforward method to fabricate polymer nanocomposite in a large scale. The method is applicable to thermoplastics, which has ability to melt and re-shape, it is further suitable for the polymers that cannot processed with solution techniques owing to their insolubility with solvents [35]. The bulk polymers could be process by several melt processing techniques such as extrusion. Particularly twin-screw extrusion, which applies intensive shear mixing, were used to produce nanofiller reinforced polymer composites. A wide range of polymer matrices could be used such as polyethylene (PE), PP, polyethylene terephthalate (PET), PC, where some of which were presented in Table 1.2 and even high-performance engineering thermoplastics such as PEEK, PEI, and PAEK.

**Table 1.2** : Melt processing of several polymers with various CNTs [35].

| Composition | CNTs wt fraction (%) | Tensile strength (% improvement) | Young's modulus (% improvement) |
|---|---|---|---|
| PS/Purified MWCNTs | 40 | 10 | 100 |
| HDPE/Pristine MWCNTs | 5 | 12 | 10 |
| LDPE/Pristine MWCNTs | 10 | 56 | 89 |
| PP/Modified MWCNTs | 1 | 10 | Not given |
| PA/Purified MWCNTs | 1 | -20 | 15 |
| PET/Pristine SWCNTs | 0.1 | 9 | 20 |

Socher *et al.* [36] studied on polymer viscosity impact on multi-walled CNTs dispersion and thus electrical properties of nanocomposites. To achieve that, the researchers worked on various thermoplastics with different grade melt viscosities. The selected thermoplastics contain both commodity and high-performance polymers, which were PA, PET, PC, PEEK and low-density polyethylene (LDPE). Electrical conductivity results revealed that increase in melt viscosity led to also increase in percolation threshold. For instance, percolation thresholds of PC are 0.5-0.75 wt % (low viscosity), 0.75-1 wt % (medium) and around 1 wt % CNTs (high viscosity). Also, percolation thresholds for PEEK showed similar behavior, which were 0.75 wt % (low viscosity grade), 1-1.5 wt % (medium viscosity) and 2 wt % (high viscosity). Thus, it was reported that melt viscosity of polymers has a great impact on electrical conductivity of composites and percolation threshold could be tailored by melt viscosity. The conductivity results were also supported by TEM analysis. TEM images (Figure 1.12) demonstrated clusters of CNTs agglomerates were visible in the all low viscosity matrices. In contrast, at high viscosity grades, CNTs agglomerates were apparently dispersed homogeneously. Furthermore, variation of CNTs length distribution was studied before and after the extrusion. In the TEM images of PC, in both viscosities CNTs were narrowed and in smaller length. According to reduction in CNTs length analysis, average CNTs lengths are 418 nm at low viscosity PC and 350 nm at high viscosity PC after process. As a result, in low viscosity CNTs retained 54 % of initial length whereas in high viscosity PC only 48 % of initial length of CNTs left. As a conclusion, CNTs lengths are shortened in all grade matrix viscosity.

Bangarusampath *et al.* [37] investigated PEEK/CNTs nanocomposites fabricated by twin-screw extrusion. Dynamic shear rheological characteristic of CNTs/PEEK nanocomposites showed an increase in both complex viscosity and moduli with increase in CNTs content. For nanocomposites containing higher CNTs weight fraction than 1 wt % demonstrated high shear thinning, which was understood by storage modulus indicated percolation of nanotubes at low frequencies. Morphological analysis of both field emission SEM (FESEM) and TEM revealed that CNTs were well dispersed in PEEK matrix. SEM characterization can be seen in Figure1.13 c and it demonstrated random and well-dispersed nanofillers however fibrillation of polymer was identified. TEM images (Figure1.13 a and b) provide better visualization, where apparently seen CNTs were well dispersed due to high shear forces applied by twin-screw extrusion process. Also, in high magnification TEM image, it was seen that CNTs were curled instead of being straight, thus this led to reducing the reinforcing effect. Electrical characterization revealed that percolation threshold for PEEK/CNTs composite is around 1 and 1.5 wt % CNTs. Following to 2 wt % CNTs/PEEK composite (around $10^{-2}$) S/cm, conductivity is slightly increased with addition of

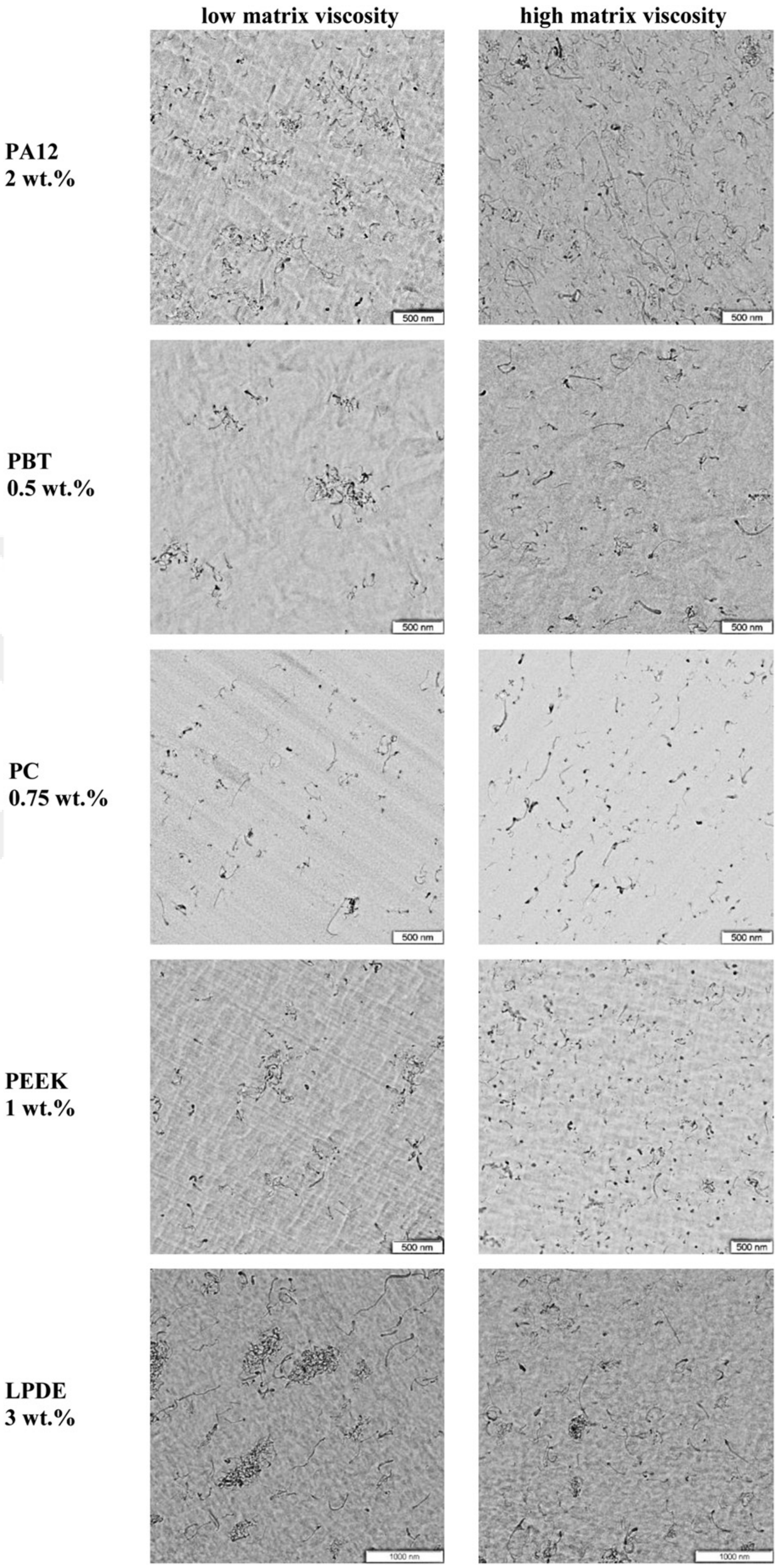


**Figure 1.12** : TEM images of CNTs dispersion in various polymers at different matrix viscosity [36].

CNTs and reached up to $10^{-1}$ S/cm for 17 wt % CNTs/PEEK. Furthermore, tensile modulus of nanocomposites increased gradually from 4000 *MPa* (for neat PEEK sample) to 6000 *MPa* (for 17 wt % CNTs/PEEK nanocomposite).

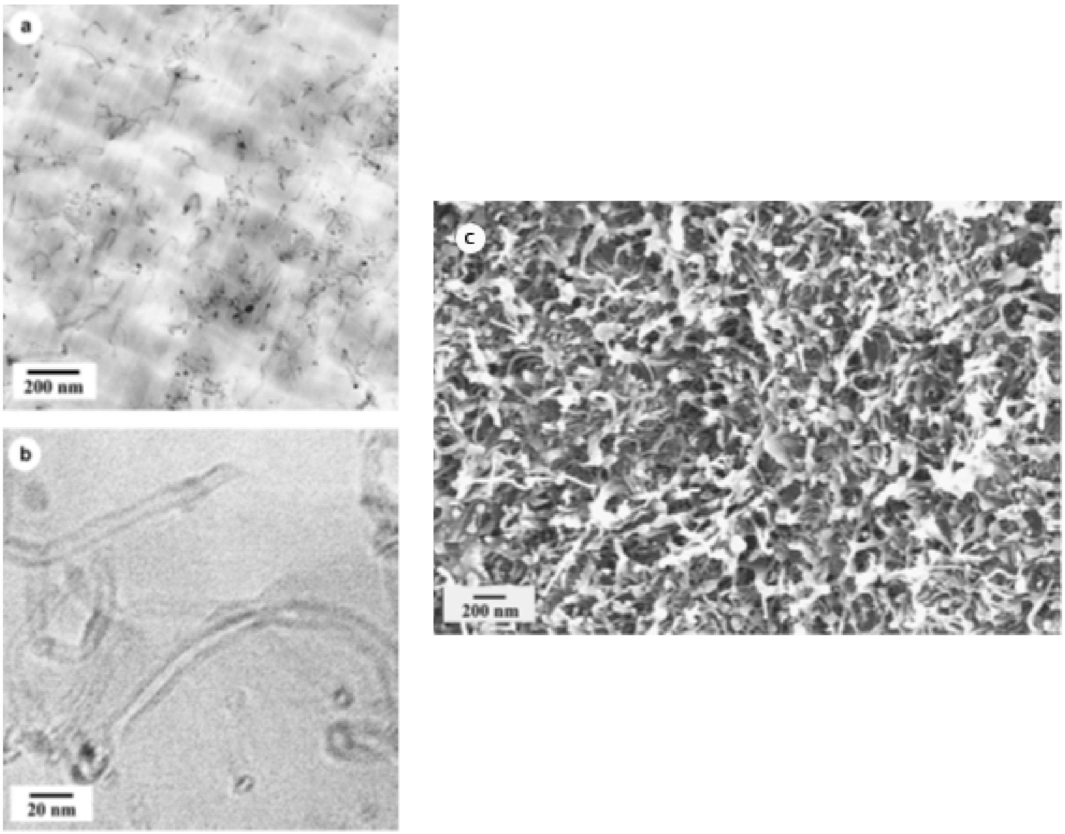


**Figure 1.13** : a) and b) TEM images and c) SEM image of CNTs/PEEK nanocomposites [37].

In the study of Isayev *et al.* [38], a novel method was developed and adopted in twin-screw extruder to improve CNTs dispersion in the high-performance polymer matrix. An ultrasonic power consumption was attached to the intermeshing co-rotating twin-screw extruder as demonstrated in Figure 1.14. The ultrasound effect was investigated by fabricating various fraction of CNTs/PEI nanocomposites ranging from 1 wt % to 10 wt %. Rheological, electrical and mechanical properties of CNTs/PEI nanocomposites were reported. Rheological results revealed that complex viscosity and shear modulus of the polymer was enormously improved by CNTs incorporation into PEI. Moreover, compared to neat samples, ultrasonic treatment resulted in an increase both in the viscosity and storage modulus. Shear thinning behavior wasn't observed in low CNTs loaded samples whereas at high CNTs loading shear thinning behavior was detected, which was indirectly related to homogeneous

CNTs dispersion in PEI matrix. Furthermore, the tensile strength of nanocomposite samples was affected by ultrasonic amplitude. The tensile strength of 10 wt % CNTs/PEI nanocomposite samples at 4 $\mu$m amplitude reached 123 MPa while the strength of 115 MPa was seen in case no ultrasonic treatment was applied. However, at high amplitudes such as 5 and 6 $\mu$m, reduced tensile strength at all fraction of nanocomposites was reported. Electrical conductivity of nanocomposites wasn't affected by ultrasonic treatment as of rheology and mechanical properties. Volume conductivity of nanocomposites reached to $5x10^{-5}$ S/cm for 10 wt % CNTs/PEI nanocomposites whereas it showed $10^{-12}$ S/cm for neat PEI.

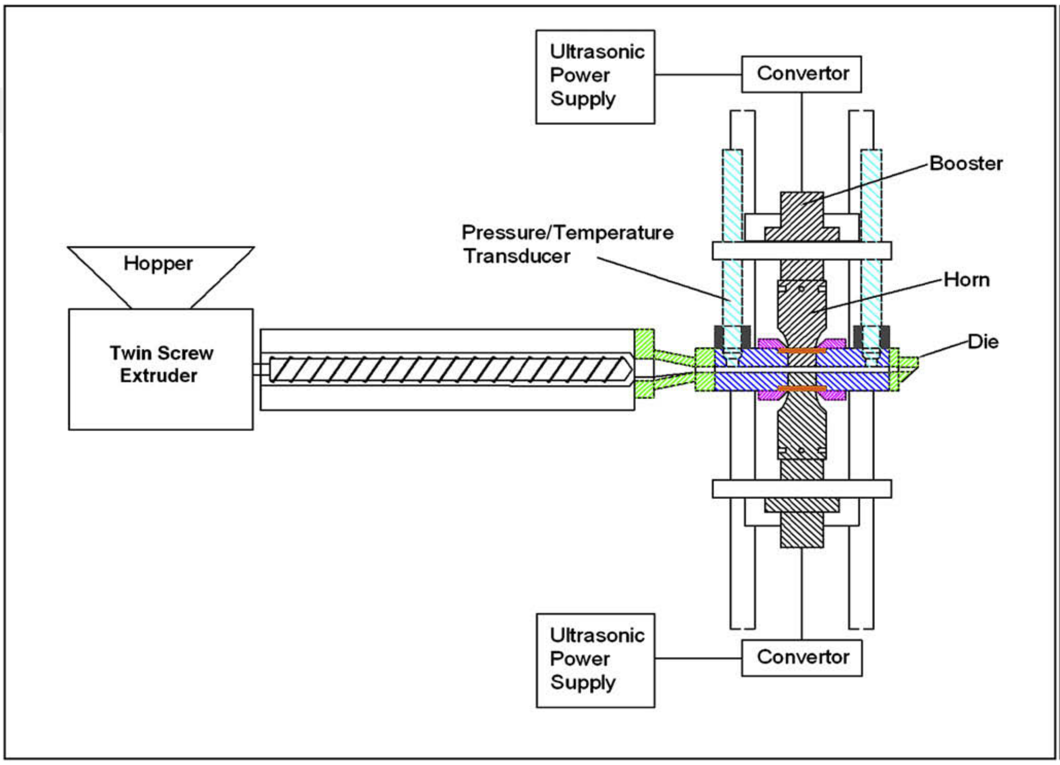


**Figure 1.14** : Ultrasound assisted twin-screw extruder [38].

In another research study [39], solely acid and plasma treated multi-walled CNTs/PEI nanocomposites were investigated under mechanical and thermal properties. The aim of surface treatment was to improve adhesion between CNT and polymer; hence improved dispersion of CNTs in polymer matrix was expected. Prior to melt compounding process, polymer and CNTs were dry mixed with a high-speed mixer to improve wetting between polymer and nanofiller. The functionalized CNTs/PEI nanocomposites were fabricated by twin-screw extruder and nanocomposite pellets were produced. It was also reported that trisnonylphenylphosphite (TNPP) stabilizer was used during extrusion process. These pellets then were fed to injection molding. In the research paper, it was repeated for several times that PEI powder was dried in a vacuum oven before any process, which was the prime drawback of PEI. The mechanical results indicated that tensile strength of plasma treated CNTs/PEI nanocomposites was increased with CNTs incorporation improved up to 11 % (114 *MPa*) and 15 % (117 *MPa*) for 0.5 and 2 wt % plasma threated CNTs/PEI nanocomposites, respectively. However, tensile strength of acid-treated CNTs/PEI nanocomposites was improved less than those with plasma treated samples, and revealed tensile strength of 7.1 % (109.8 *MPa*) and 6.9 % (109.6 *MPa*) for 0.5 wt % and 2 wt % COOH-CNTs/PEI samples respectively. As a reason, the scholars claimed that plasma treated CNTs had better wettability properties with PEI compared to chemical treated CNTs. Differential scanning analysis (DSC) highlighted that $Tg$ of neat PEI was around 217°C. Incorporation of solely 2 wt % plasma treated CNTs/PEI and COOH-CNTs/PEI resulted in slight shift in $Tg$ of 227°C and 221°C respectively. As they reported, this result triggered by plasma treated CNTs/PEI nanocomposites' better wettability and lack of chain mobility due to reduced interfacial adhesion. Furthermore, general trend of increase in $Tg$ with CNTs incorporation suggested efficient interfacial adhesion between treated nanofillers and polymer. Thermogravimetric analysis showed maximum decomposition temperature increased by CNTs addition up to 579°C for 2 wt % plasma treated CNTs/PEI nanocomposites, which was 528°C for neat PEI sample. FE-SEM characterization demonstrated less agglomeration of plasma treated CNTs/PEI nanocomposites than COOH-CNTs/PEI samples. Furthermore, HRTEM supported that observation. Untreated CNTs/PEI images had high agglomeration than treated CNTs/PEI composites. Also, agglomeration in plasma CNTs within PEI was less than COOH-CNTs/PEI. This result also strengthened high tensile strength of plasma treated CNTs/PEI nanocomposite, which indicated efficient load bearing capability, high interfacial adhesion and effective treatment.

#### 1.1.4.2 Nanocomposite filaments for FDM applications

Structural nanocomposite materials fabricated by additive manufacturing has gained noticeable attention due to offering to tailor the material characteristics of 3D printed objects and thus leading to various multifunctional properties [1, 40]. Despite

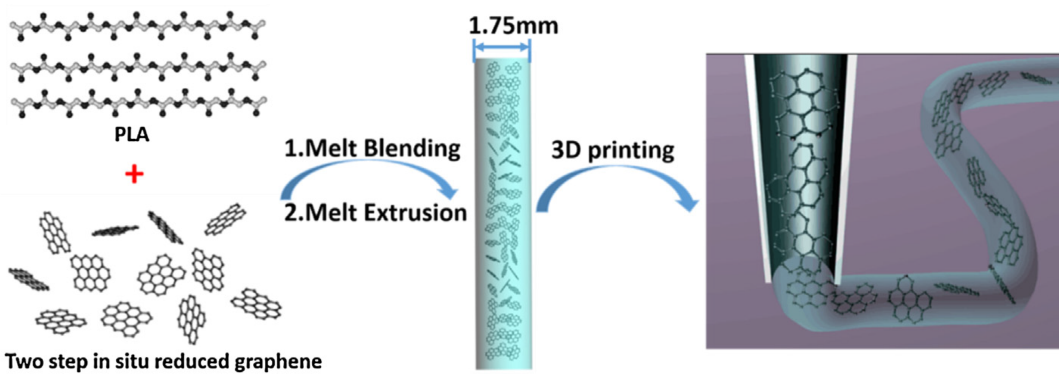

**Figure 1.15** : r-GO/PLA filaments fabrication and 3D printing [41].

the potential of multifunctional FDM filaments, there exist a few research studies of nanocomposite filament fabrication in the literature. Zhang *et al.* [41] have investigated the fabrication and AM application of the reduced graphene oxide (r-GO) reinforced PLA FDM filament with a standard diameter of 1.75 mm. The process of graphene/PLA filaments is demonstrated in Figure 1.15. The results revealed that 6 wt % r-GO/PLA samples had approximately 4.75 S/cm in electrical conductivity. In addition, 6 wt % r-GO/PLA 3D printed samples demonstrated two-fold improvement compared to neat PLA samples in terms of tensile strength which reached up 65 MPa. However, 8 wt % r-GO/PLA samples showed a brittle structure which indicated that composite rigidity was too high.

Then, Gnanasekaran el al. [42] reported solely graphene and CNTs reinforced polybutylene terephthalate (PBT) filament feedstocks. The study revealed that electrical percolation threshold of CNTs/PBT (0.31 vol. %) was lower than graphene/PBT's (3.3 vol. %) due to changes in filler dimension from 1D CNTs to 2D for graphene and, the possibility of graphene agglomeration and trapped air in exfoliated flakes. The researchers also highlighted that 3D printed structures of CNTs/PBT showed better functional properties of both mechanically robust objects and electrically conductive. Furthermore, printing conditions of reinforced PBT didn't vary compared to neat PBT printing since very low vol. % filler was incorporated into the polymer matrix.

In a very recent study, Dul *et al.* [43] fabricated CNTs/ABS nanocomposite filaments from 1 wt % to 8 wt % and revealed the effect of CNTs on electrical conductivity and mechanical performance. The results indicated that the conductivity of the filaments was improved with an increase in CNTs weight fraction up to 0.55 S/cm as of 8 wt

% CNTs/ABS filament. Also, 6 wt % CNTs/ABS filaments demonstrated the highest tensile strength among the specimens, which increased from 42 *MPa* for neat ABS filament to 47 *MPa* for those filled 6 wt % CNTs. Morphological analysis by field emission SEM (FESEM), which can be seen in Figure 1.16, were also supported to enhanced mechanical and electrical properties. The FESEM micrographs revealed that CNTs are homogeneously distributed and dispersed in ABS matrix. Also, in images at high magnifications, good adhesion between CNTs and ABS was exhibited.

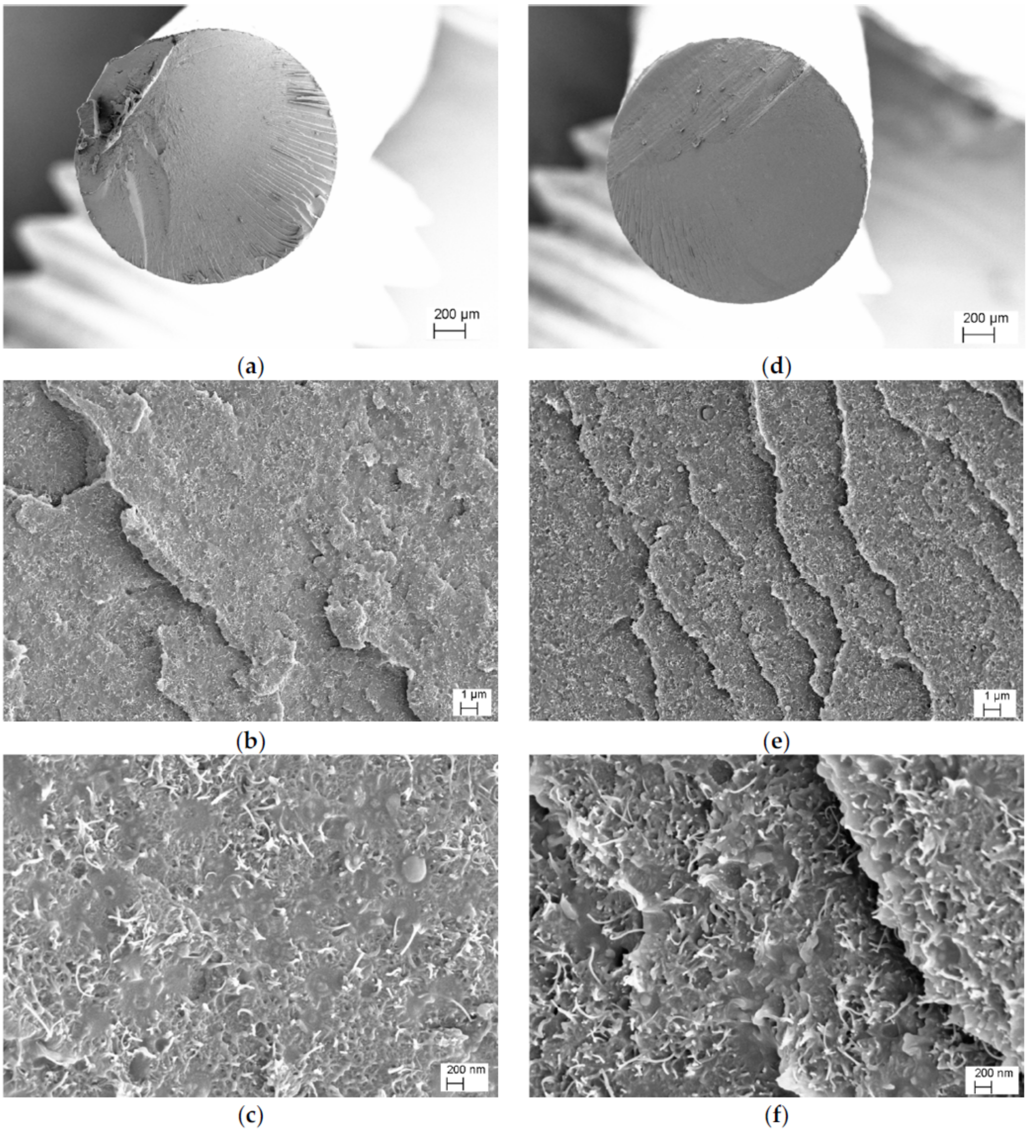


**Figure 1.16** : FESEM images of 6 (Left) and 8 (Right) wt % CNTs/ABS filaments at different magnifications. [43]

However, some application areas, particularly in aerospace, require efficient load bearing capability with low weight ratio to its strength. Though the nanofiller enhancement, these commodity thermoplastic matrices provide limited strength compared to high-performance thermoplastics such as PEEK and PEI. To the best of our knowledge, no PEI matrix composite filaments has not been reported yet even though its convenience to additive manufacturing applications [15].

Berretta *et al.* [44] investigated CNTs/PEEK FDM filaments at 1 wt % and 5 wt % nanofiller weight fractions. They reported that 5 wt % CNTs/PEEK filament demonstrated a slight improvement in ultimate tensile strength reached up 105 MPa from 100 MPa for neat PEEK filaments. Morphological studies by TEM revealed that CNTs were well distributed in PEEK matrix, which 5 wt % CNTs/PEEK filament's morphology can be seen in Figure 1.17. However, well-dispersed CNTs morphological results didn't match with tensile test results, which was not discussed. Also, there was not any description on the changes in electrical properties of nanocomposite filament or 3D printed samples.

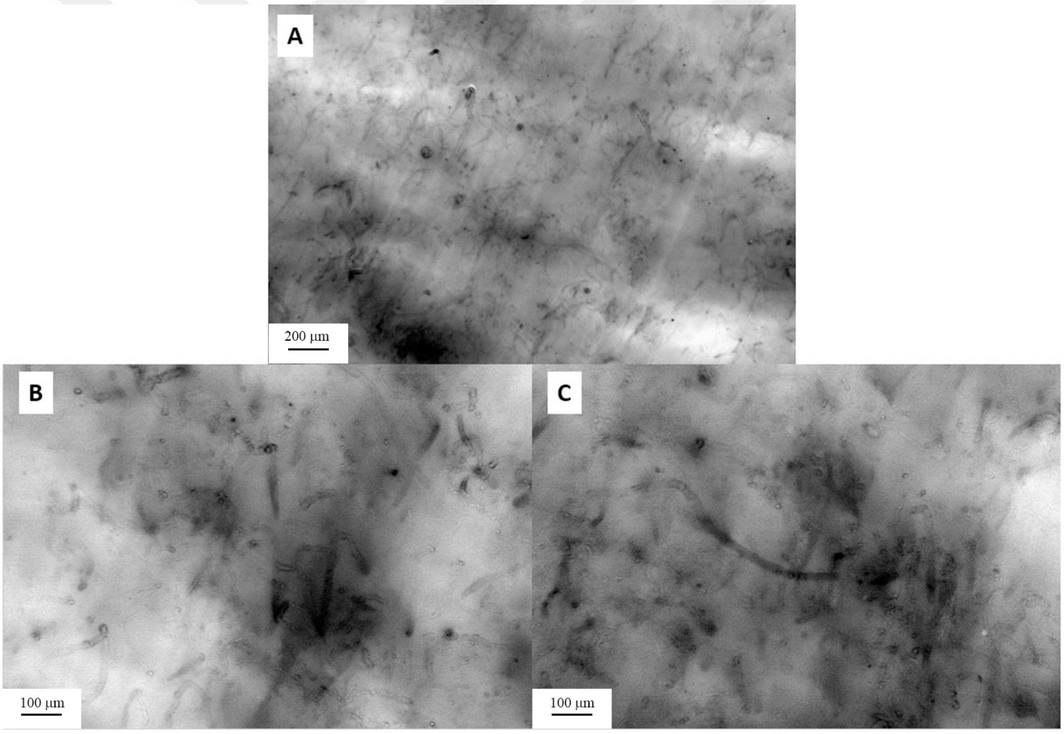


**Figure 1.17** : TEM images of 5 wt % CNTs/PEEK filament at different magnifications [44].

## 1.2 Motivation

Additive manufacturing or 3D printing is an emerging process to create 3D shaped structural components, which eliminates post-processing such as cutting, trimming. Among several polymer filaments in 3D printing, multifunctional and strong thermoplastic filaments offer new possibilities for many industries including aerospace, architecture, automotive, defense, and among many others. Particularly in the aerospace industry, high-performance thermoplastic polymers PEEK and PEI based laminated composites, are the leading the market when high temperature resistant up to 200 °C, high tensile and impact strength and light weight are needed [15]. 3D printers might have significant impact, which facilities complexity reduction in manufacturing. Nevertheless, another emerging technology called "Metal 3D printing" also enables the fast, accurate and cost-effective production of high-performance metals. When specific density and specific strength are design concerns, polymeric structures come to the forefront. A variety of manufacturing techniques in polymer processing, when blended with tailoring microstructure and chemistry, creates unique structures. In this thesis, the hypothesis is that the incorporation of stiff and strong carbon nanotubes into PEI matrix results in significant improvement both in mechanical and electrical properties. This enhancement is attributed to combined effect of dispersion state of CNTs and their compatibility of PEI matrix. There has been still challenges in the processing of high-performance polymers due to their high viscosity and required high extrusion temperatures. This traces the effect of CNTs on melt-processing of PEI filaments specifically designed for 3D printing. A series of melt-processing methods are used to fabricate electrically conductive and strong CNTs/PEI filaments. This thesis also addresses the underlying challenges in CNTs/PEI extrusion and ultimately points out the process design requirements for continuous CNTs/PEI filament production. The next step of this research will focus on the production of cellular polymer nanocomposite structures, which is possible by using a 3D printer with a high-temperature nozzle and controlled environmental chamber for good quality printing.

### 1.3 Road Map of Thesis

In this thesis, neat PEI and CNTs/PEI filaments were fabricated to be utilized as feedstock in 3D printers. The neat and nanocomposite filaments were produced by using a combination of twin and/or single-screw extruders, which were specifically designed by us to process high performance engineering polymers including PEI. Figure 1.18 demonstrates neat and CNTs reinforced PEI filaments were successfully

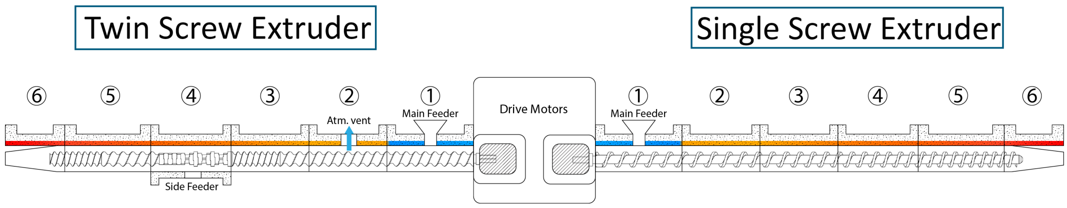

**Figure 1.19** : Diagram of twin and single-screw extrusion.

fabricated in a continuous manner. While, neat PEI filaments could be processed through single-screw extruder, a series of melt processing steps was required for nanocomposite filament production. In CNTs/PEI filament fabrication, PEI granules were fed through main feeder of twin-screw extruder in which CNTs were fed by using side feeding head as demonstrated in Figure 1.19. Then, another twin and single-screw extrusion step was employed consecutively for homogenous dispersion. The nanocomposite strands were cut into granule size by a granulator. This twin-screw extrusion process and later granulation were repeated at least three times to ensure homogeneous dispersion of CNTs in PEI matrix. Then, these nanocomposite granules were fed to main feeder of single-screw extrusion, and the molten CNTs/PEI was extruded to form filament. In conclusion, a standard diameter of FDM nanocomposite filaments with standard diameter of 1.7 mm were fabricated and characterized in terms of their mechanical and electrical properties.

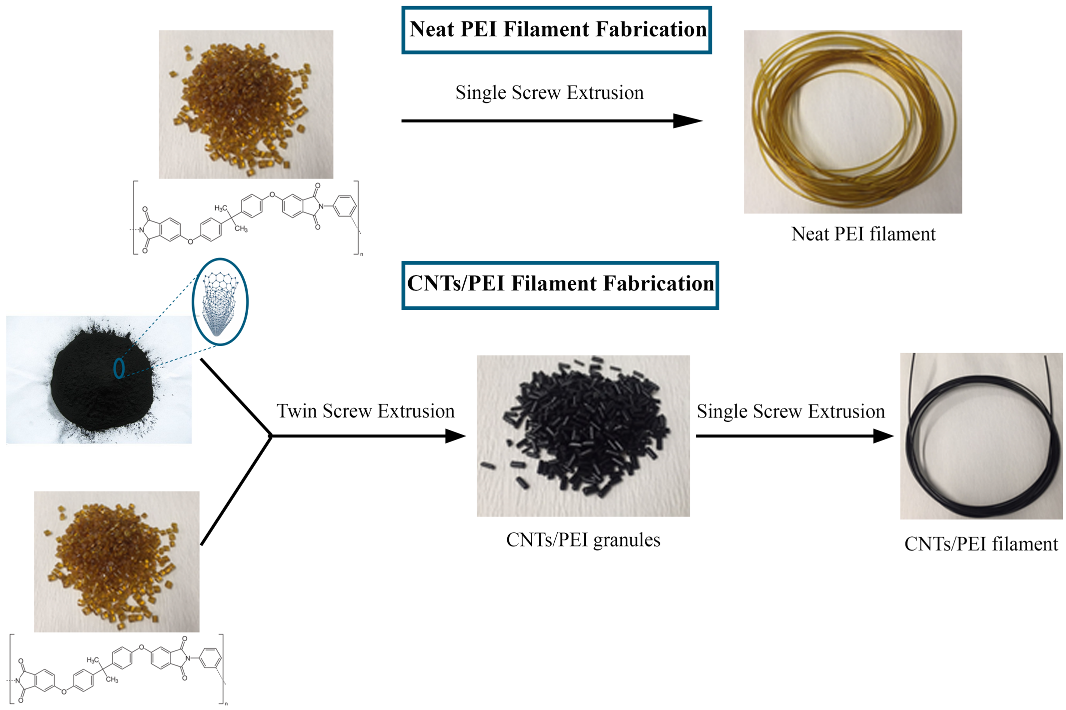

**Figure 1.18** : Road map of neat PEI and CNTs/PEI filament fabrication.

# 2. MATERIALS AND METHODS

## 2.1 Materials

PEI (benzene-1,3-diamine;5-[4-[2-[4-[(1,3-dioxo-2-benzofuran-5-yl)oxy]phenyl]propan-2-yl]phenoxy]-2-benzofuran-1,3-dione) amorphous thermoplastic was used for polymer matrix. The PEI pellets (Tecotek® EI20 NL) were purchased from Eurotec (Tecotek EI20 NL). In the technical data sheet, it was reported that density of PEI is 1.27 $g/cm^3$, molecular weight is 592 $g/mol$ and $Tg$ is 217 °C. N-Methyl-2-pyrrolidone (NMP, $C_5H_9NO$ 1-Methylpyrrolidin-2-one UIPAC and molecular weight of 99.13 g/mol, N,N-Dimethylacetamide (DMAc, $C_4H_9NO$) with 87.12 g/mol, dimethylformamide (DMF, $C_3H_7NO$) with 73.09 g/mol and ethanol ($C_2H_6O$) with 46.07 g/mol molecular weight was purchased from Sigma-Aldrich was used without further purification.

### 2.1.1 Carbon nanotubes (CNTs)

CNTs were purchased from Nanokomp MWCNTs, Carbon purity: min. 90%, Diameter: 5-15nm, Length: 1.5-2$\mu$m), used as reinforcing filler for the nanocomposite filaments. .

## 2.2 FDM Filament Fabrication

### 2.2.1 Neat PEI filament fabrication

Before the extrusion processes, the extruders was needed to be purged. Purging was first carried out by PP. However, it was seen that PP couldn't pushed leftover PEI from previous process. This led to burning of PEI/PP leftover in the process and that was understood by converting neat PEI in black color (which should be in yellow-orange color). Our experiments and Mittal *et al.*'s [23] study revealed high density polyethylene (HDPE) was the best purging polymer for PEI application in melt process. Hence, it was noted that following to HDPE purging, no burning in the filament surface was observed.

Neat PEI filament was directly fabricated by single-screw extrusion without using any additives or lubricant. The main drawback of PEI was the ability to absorb moisture. This led to obtain porous structure inside filament structure during extrusion. Thus, PEI pellets were dried in a vacuum oven at 150 °C for at least 2 hours to ensure dehumidification. Neat PEI filament fabrication was performed by using single-screw extruder. The barrel temperatures were set at 310, 330, 340, 350, and 360 °C. The screw speed was arranged at 100 rpm. Neat PEI pellets were fed by the hopper. To fabricate filament with a standard diameter, molten polymer from extruder die was drawn at 3 rpm to obtain filament stable with 1.70 mm diameter.

### 2.2.2 CNTs/PEI nanocomposite filament fabrication

#### 2.2.2.1 Melting of PEI granules before extrusion process

These low weight and fluffy CNTs have tendency to agglomerate and thus it was difficult to disperse CNTs in a polymer matrix. Hence, to maintain weight fraction of CNTs in PEI matrix, it was first considered to melt the PEI and then incorporate CNTs into molten polymer. To achieve this, the polymer pellets or powders were collected into a circular beater and heated in a mantle heater. However, due to high viscosity of PEI and PEEK, the process was unsuccessful where the polymers could not melt efficiently. Instead, polymer started to degrade due to inefficient magnetic mixing. Then, solution mixing was proposed to overcome this issue.

#### 2.2.2.2 PEI/CNTs mixing strategies

**Solution mixing of CNTs and PEI blends**

CNTs reinforced PEI or PEEK filaments were considered to be developed for 3D printing applications. Due to solubility difficulties of PEEK polymer, sulfonated PEEK (s-PEEK) is also considered as an alternative matrix for the filament. Fabrication of composite polymer/nanofiller pellets was performed by using twin-screw extruder to achieve sufficient CNTs dispersion.

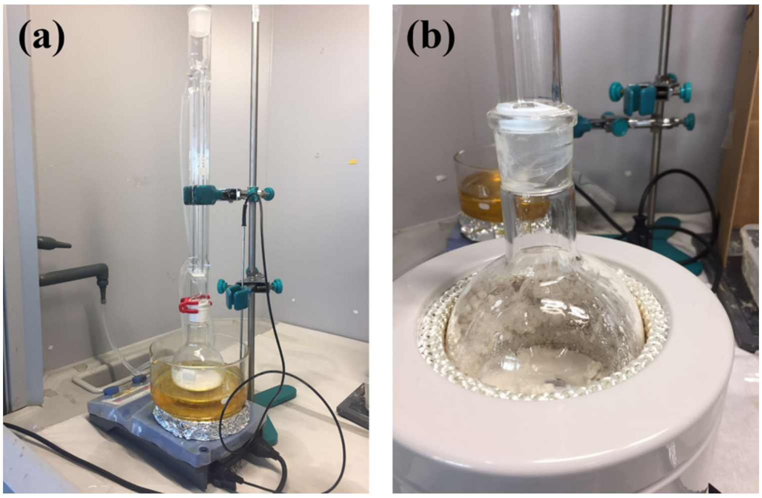


**Figure 2.1** : Reflux system process (a) oil and (b) mantle based, where heating was provided from bottom through oil and continuously through the whole ball, respectively.

Due to the agglomeration tendency of CNTs, both incorporation and dispersion of them through matrix were difficult. Firstly, high density gel formation of PEEK polymer was investigated experimentally by dissolving in DMF solvent via reflux system as seen in Figure 2.1 in order to prevent CNTs agglomeration while feeding through the twin-screw extruder. Two types of reflux systems were used in this thesis, which were stirring oil base and mantle. The restriction of oil-based stirrer was not to rise high temperature limited up to 170 °C. Several concentrations of PEEK in DMF solution were experimented. The main problem high concentration PEEK/DMF solution during refluxing was chemical resistivity of polymer itself and mixing inefficiency where the solution spread through the walls of circular flask. The issue was tried to overcome either increasing amount of solution without disturbing the ratio of solution or decreasing mixing rpm. However, neither worked to solve the problem.

s-PEEK was also dissolved in DMF at room temperature and mixed via magnetic stirrer by gradual addition method. Following to complete dissolution of s-PEEK in DMF, CNTs addition into s-PEEK/DMF solution was performed. Then, the solution was dried until the solvent completely removed.

Hansen solubility parameters were guided to determine an efficient way to solve PEI. Regarding Hansen solubility parameters of $\delta_d$, $\delta_p$ and $\delta_H$ corresponding to dispersion forces, polarity, and hydrogen bond interaction, respectively, which could be seen in Table 2.1, NMP and Dimethylacetamide (DMAc) were promising as a solvent for

**Table 2.1** : Hansen Solubility Parameters of solvents and materials [47].

| Polymer/Solvent | $\delta_d$ | $\delta_p$ | $\delta_H$ |
|---|---|---|---|
| PEI | 19.6 | 7.6 | 9 |
| NMP | 18 | 12.3 | 7.2 |
| DMAc | 7.87 | 11.5 | 10.2 |
| MWCNT | 18.5 | 7 | 4.8 |
| Ethanol | 15.8 | 8.8 | 19.4 |

homogeneous PEI and CNTs solution. For the selection of good solvent, evaporation rates of NMP and DMAc were considered. When ether equals to 1, evaporation rates of NMP [45] and DMAc [46] are 360 and 172, respectively. As a conclusion, NMP was decided to dissolve for PEI and disperse CNTs solution to evaporate effectively, which was experimentally confirmed as seen in Figure 2.3. Besides, ethanol was determined as a solvent to precipitate PEI/CNT granules.

PEI/CNTs/NMP solution was simply prepared by stirring magnetically. PEI/NMP and CNTs/NMP solutions were prepared separately and then the homogeneous solutions were mixed and stirred magnetically. The processes were performed at room temperature. Weight fraction of CNTs was determined as 10 wt % of PEI for all the solutions

Pellet precipitation was carried out by dropping CNTs/PEI solution into the solvent which the polymer coagulated immediately when it interacted with solvent molecules. The pellets were fabricated through the thin glass pipettes without any additional force but gravitational force. As it could be seen in Figure 2.2, to accelerate the granulation process, multiple pipettes were placed where a holder which was 3D printed holder designed according to fitting diameter of glass pipettes.

As Figure 2.3 (a) and (b) clearly reveals that smaller diameter of PEI/CNTs/solvent granules were produced due to the evaporation of the solvent. This indicates efficient evaporation of the solvent presented in the pellets.

Evaporation of NMP solvent was performed at 180°C for 12 hr in a vacuum ovet to ensure complete drying whereas DMAc was evaporated at 160°C for 12 hr. Finally, small diameter PEI/CNT granules were obtained as seen in Figure 2.4.

In several recent works [39, 48], CNTs/polymer granules were fabricated prior to melt extrusion process due to CNTs intention to agglomerate. However, manual control

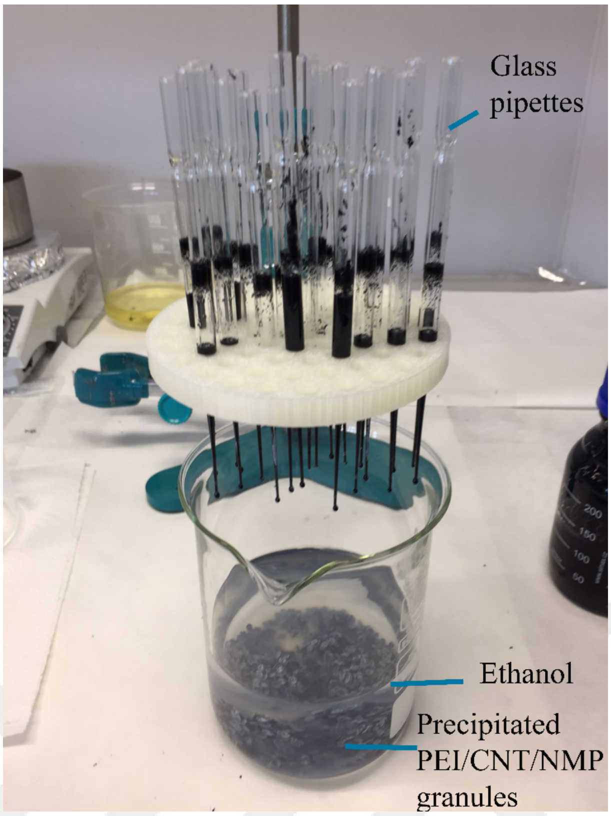


**Figure 2.2** : Fabrication of PEI/CNT/NMP granules by precipitation in ethanol solvent.

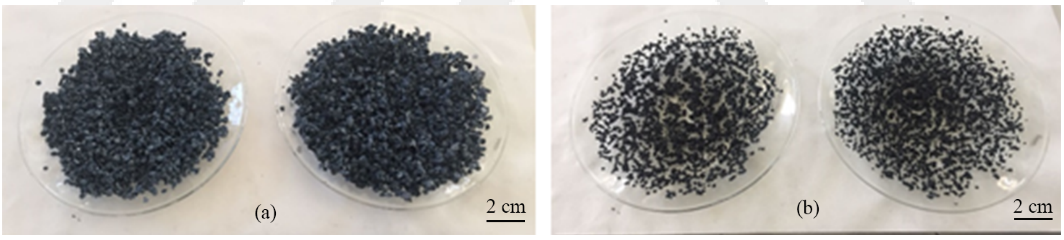


**Figure 2.3** : Diameter differences of (a) before and (b) after the solvent evaporation in vacuum oven.

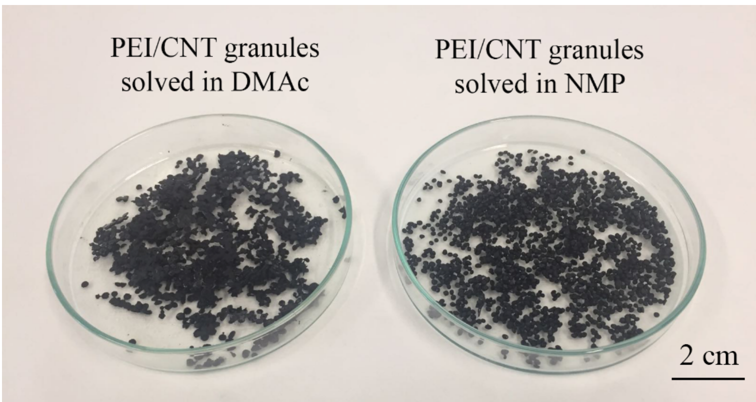


**Figure 2.4** : Comparison of CNTs/PEI granules solved in DMAc and NMP. The granules of former were slightly adhered to each other while the letter granules were separated.

technique raised process obstacles such as polymer congress in the glass pipettes and longer process time. Thus, these difficulties led to design a much simple use method for pelletizing. The method simply consisted of four parts as seen in Figure 2.5. The configuration of the needles used Nippon's design specifically for wet spinning, which was demonstrated in Figure 2.5 b. To overcome surface tension of PEI/CNTs/NMP solution in the tip of needles, controlled gas pressure was applied during precipitation into ethanol solvent. Compared to glass pipettes, tip diameter of the needles was %50 smaller and designed pelletizing tool contains 361 needles, which number was much larger than the glass pipetting system since maximum only 15 pipettes could be manually controlled during the process. Thus, process time significantly decreased from 3 days to 30 minutes when the same volume of CNTs/PEI solution was dispersed by using pelletizing tool.

Despite proving significant advantages, pelletizing tool has brought a few problems. First, size of precipitated (or encapsulated) CNTs/PEI pellets were with miscellaneous dimensions as demonstrated in Figure 2.6. Besides, some of the pellets were much larger which made it difficult to complete evaporation of the solvent molecules. In fact, NMP residues trapped inside pellets were also detected by Thermal Gravimetric Analysis (TGA) analysis. That caused significant gas outlet during extrusion processes as demonstrated in Figure 2.8 and defects and inconsistencies in filament properties such as its stiffness, brittleness and surface roughness. Thus, recently the studies were focused on overcoming the evaporation issue of NMP and several solutions proposed as:

- Drying pellets either for longer periods or at higher temperatures (or both)
- Making powder from CNTs/PEI pellets and post-drying them

However, these proposed solutions did not lead to effective solvent evaporation. In addition, working difficulties of pelletizing tool could not be overcome. The main difficulty of pelletizing tool was agglomeration of polymer/CNTs solution from several dies. This led to huge encapsulated droplets and clogging in many dies as demonstrated in Figure 2.7. Thus, alternative method was developed without using solvent or any additives.

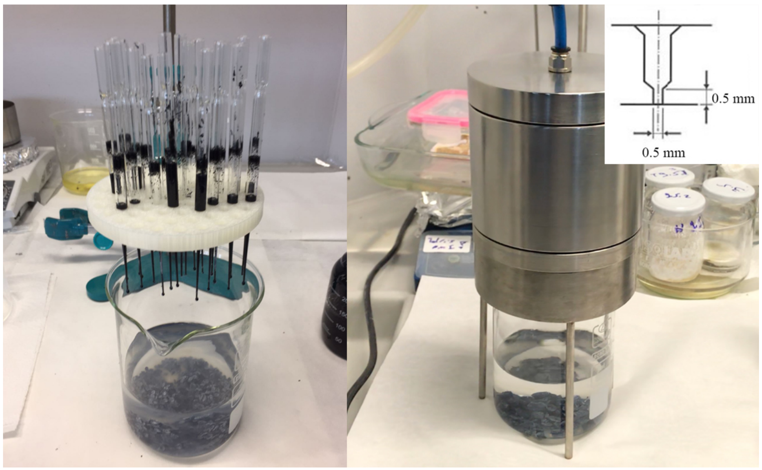


**Figure 2.5** : Fabrication and precipitation of CNTs/PEI pellets by a) glass pipettes and b) pelletizing tool with needle configuration.

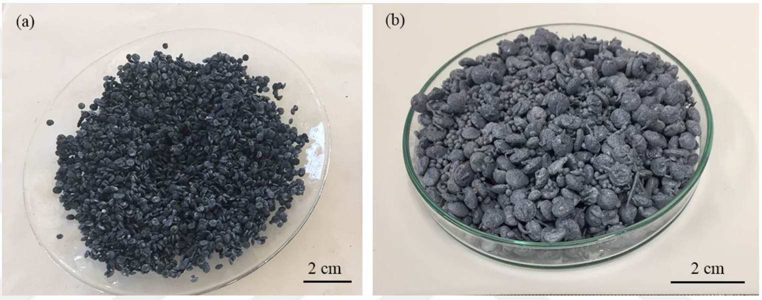


**Figure 2.6** : CNTs/PEI pellets fabricated by a) glass pipettes and b) pelletizing tool.

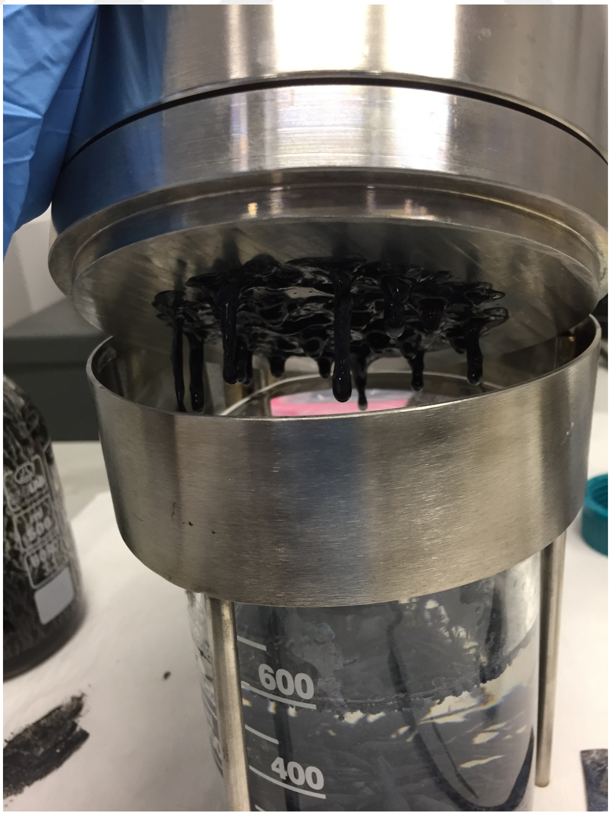


**Figure 2.7** : Solution agglomeration problem of pelletizing tool during CNTs/PEI pellet encapsulation.


**Figure 2.8** : Gas outlet during extrusion process of CNTs/PEI pellets due to solvent molecules.

**Feeding of CNTs and PEI granules for mixing**

In the solution mixing method, the motivation was that to maintain the exact CNTs weight percent in PEI matrix. However, due to working difficulties and inefficient outcomes, we preferred directly feeding polymer and CNTs through the extruders. Moreover, the results section in this thesis demonstrated the improvement in both tensile behavior and conductivity characterizations as CNTs weight fractions increased. Thus, we could conclude that the weight loss during direct feeding process was ignored.

In addition to fabricating filament from CNTs/PEI pelleting, direct feeding system of solely CNTs (from side feeding) and PEI granules (from the main feeding) to the extruder was investigated to reveal CNTs effect on both electrical and mechanical performance of the FDM filaments as seen in Figure 2.9. In this system, PEI granules were fed from the main feeding while CNTs were dispersed from side-feeder of twin-screw extruder. After first extrusion process, nonhomogeneous CNTs/PEI filament was cut into granule sizes then twin-screw extrusion was processed for five times to ensure a homogeneous mixture. Following to twin-screw extrusion processes,

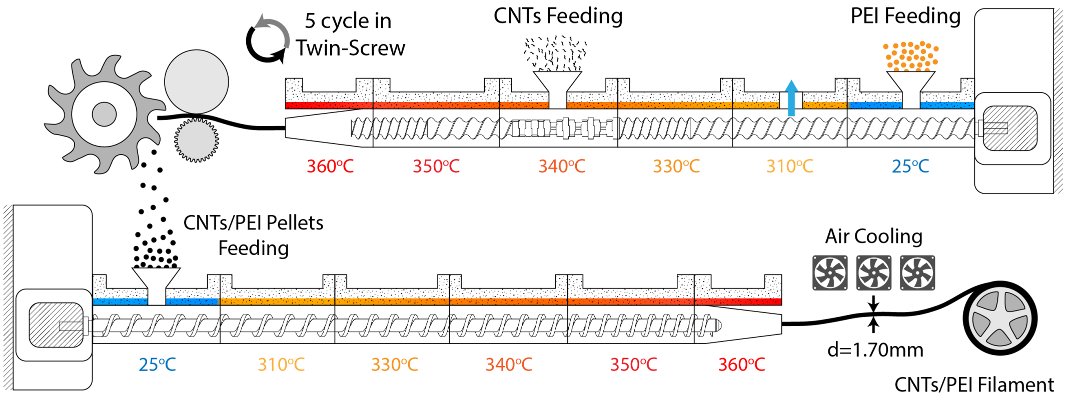


**Figure 2.9** : Fabrication processes of CNTs/PEI filament by extrusion at ITUARC.

single-screw extrusion was applied to fabricate unique diameter nanocomposite filament.

The CNTs/PEI filament fabrication began with desiccating PEI polymer in a vacuum oven for at least two hours at 150 °C. Following dehumidification of PEI, twin-screw extrusion was processed. In the twin-screw extrusion process, PEI fed by main feeder is marked in Figure 2.9 and at the same time CNTs were fed by side feeder. Then, the output nanocomposite strand from twin-screw extruder was cut into pellet size by a cutter to feed the nanocomposite pellets repetitively. To ensure homogeneous dispersion and distribution of CNTs, the twin-screw extrusion process applied to nano-mixture for five times. The resultant CNTs/PEI nanocomposites were cut into pellet size to later feed them through single-screw extruder. Co-rotating twin-screw extrusion provided higher shear stress to the mixture compared to single-screw extruders. Thus, primary homogeneous mixing of CNTs and PEI was obtained by twin-screw extrusion. The barrel temperatures of the process were set as 310, 330, 330, 340, 350 and 360 °C for CNTs/PEI nanocomposites and the screw speed was set at 100 rpm.

Following to twin-screw extrusion, CNTs/PEI nanocomposite pellets then were processed in single-screw extruder to form as filament homogeneously. The pellets were fed through single-screw extruder at 100 rpm with 310, 330, 330, 340, 350 and 360 °C barrel temperatures. The process was carried out for one cycle. The diameter of the filament was optimized by either optimizing drawing speed or fixing the outlet pressure of single-screw extruder. The output filament was drawn to be later used in 3D printing applications. The fabricated filament samples could be seen in Figure 2.10.

**Figure 2.10** : a) CNTs/PEI and b) neat PEI filament.

## 2.3 Characterization Methods

### 2.3.1 Thermal analysis

#### 2.3.1.1 Differential scanning calorimetry

Differential Scanning Calorimetry (DSC) is a thermal analysis method to determine change of materials' heat capacity by temperature. According to mass changes when heated or cooled, the heat capacity is monitored by variation in the heat flow. Thus, this leads to identify phase transitions such as melt, glass transition, phase changes and curing [49]. DSC has ability to analyze various materials including polymers, food, printing, agriculture, electronics. For the polymeric materials, glass transition temperature $(Tg)$ is significant to identify the material. Usually DSC analysis on polymers are performed by heating from room temperature to above melting temperature. Melt crystallization of polymers was carried out by several DSC runs, which are heating, cooling and reheating [50]. DSC analysis were carried out by using DSC 4000 Perkin Elmer equipment (Waltham, MA, USA), which samples with about 6 mg under a nitrogen flow of 20 mL/min. The specimens were analyzed by two cycles from 50 °C to 350 °C at a rate of 10 °C/min. Second cycle was excepted as essential for this thesis.

#### 2.3.1.2 Thermogravimetric analysis

Thermogravimetric analysis (TGA) is a thermal analysis method to investigate degredation properties of various materials. TGA supplies complimentary and supplementary data to DSC analysis. TGA detects the amount and rate change in a known mass of a specimen as an either temperature function or time at controlled temperature [51]. TGA is used for determination of thermal and degradation properties of materials and compositional features of the samples. Materials are analyzed by exhibiting mass gain or loss when decomposition, oxidation or loss of volatiles occur. TGA is specifically useful for polymeric materials. TGA can be performed under either air or nitrogen atmosphere. In addition, TGA reveals information about material selection for a specific application and prediction of product performance.

TGA was conducted in this study to reveal neat PEI and CNTs/PEI filaments' thermal and oxidative stabilities, decomposition kinetics, moisture content and filler content of materials. Thermal degradation behavior was performed through a Exstar TG/DTA7200 (RT Instruments, Woodland, CA, USA). The mass of the samples are about 8 mg and the analysis were performed from 30 °C to 800 °C at a rate of 10 °C/min in an air flow of 2 mL/min.

### 2.3.2 Morphological analysis

#### 2.3.2.1 Scanning electron microscopy

Scanning electron microscopy (SEM) is a surface characterization method, which include a beam of focused electrons with relatively low energy. SEM consists of an electron source, electromagnetic lenses, electron detectors, sample chambers and computer, as seen in Figure 2.11. The generated electrons where at the top of the column are gone through downward by passing a group of lenses and apertures, which lead to obtain a fine beam of electrons [52]. The movable electron beam scans the sample surface under vacuum. This electron beam provides information about a defined area of the sample surface. The interaction of the electron beam and the sample lead to producing various signals, which could then be detected by appropriate detectors. SEM provides three-dimensional visualization of sample surface in detail.

Sample preparation before SEM process is essential. Samples are cut to fit 1 mm x 1 mm holder where includes 6 holders. Before the process, the non-conductor specimens were coated with gold or carbon to make the sample surface conductive.

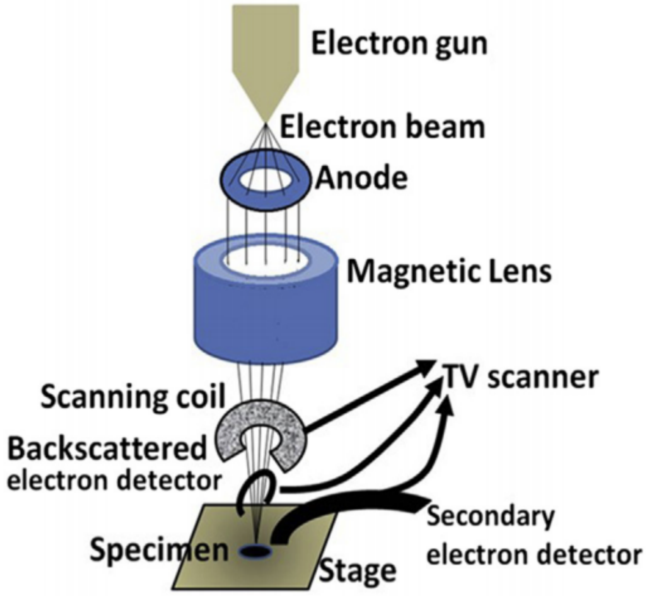

**Figure 2.11** : SEM working principle [52].

The morphologies of 5 and 7 wt % CNTs/PEI filaments were evaluated by imaging using 15 keV secondary electrons in field-emission gun equipped scanning electron microscope (SEM, LEO 1530VP). The specimen filaments were fractured in liquid nitrogen.

#### 2.3.2.2 Transmission electron microscopy

Transmission electron microscopy (TEM) is a characterization method that enables the transmission of electron beams through the sample which has nanoscale thickness and various interactions between electron beam and specimen occur. The combination of high kV beams, which is available up to 400 kV, and intense electron source are included in TEM [53]. TEM is eligible to use in various areas such as biology, biomedical, crystallography and polymers. TEM offers to identify the sample atomistic structure because electrons are smaller than atoms. The image resolution of TEM equals to approximately half of light wavelength. Best resolution of TEM could be calculated by;

$$S = 1.22\lambda/\beta \tag{2.1}$$

Where $S$ is the smallest distance can be resolved, $\lambda$ is wavelength and $\beta$ is semi-angle of magnifying lens correlation. TEM resolution is well below the 0.1 nm.

Sample preparation for TEM is a crucial step since results by TEM are directly influenced by specimen. The sample should be thin enough to enable electron transfer through specimen. Specimen preparation method varies depending on the material type. Several methods could be used to prepare cross sectional TEM sample including mechanical polishing of specimen surface and light ion milling. However, these techniques in some cases does not satisfy TEM specimen requirements. TEM specimen in precise areas or particularly containing nanoscale particles are convenient to be prepared by focused ion beam (FIB). Then, FIB combined with SEM to obtain TEM lamellae in a specific area with special accuracy [54]. The specimen initially coated with a protective weighty metal such as platinum and tungsten to avoid damages from ion irradiation. Then, a large chunk of the specimen is cut by ion-beam milling and fixed into copper grid. By using lift-out method, the specimen sides plan to view are milled for cross sectional thinning. Following to final thinning, the sample is ready for TEM investigation [55].

In this study, 0.1 and 7 wt % CNTs/PEI filaments were investigated by TEM to reveal CNTs distribution and dispersion in PEI matrix and its impact on percolation threshold. Sample preparation was the main issue for TEM since ultra-thin specimens are required to ensure electron transport. Thus, our filament specimens with 100 *nm* thickness were prepared by FIB. The images were captured at 200 *kV* acceleration voltage.

### 2.3.3 Quasi static tensile testing of FDM filaments

Tensile properties often are used to predict the behavior of a material subjected to tensile loadings. To investigate the CNTs contribution on the nanocomposite filaments in terms of stiffness, elongation and ultimate tensile strength, tensile test as seen in Figure 2.12 was performed at room temperature by using Zwick Roell Z100 Universal testing machine (Atlanta, USA) with a load capacity of 100 kN. Since the materials were filaments, Bollard style grids were selected. Tensile properties such as ultimate stress, fracture stress were determined at a crosshead speed of 5 mm/min for at least four replicates. The specimen dimensions were length of 60 cm, gauge length of 100 mm and a diameter of 1.70 mm, which were determined according to ASTM D3379.

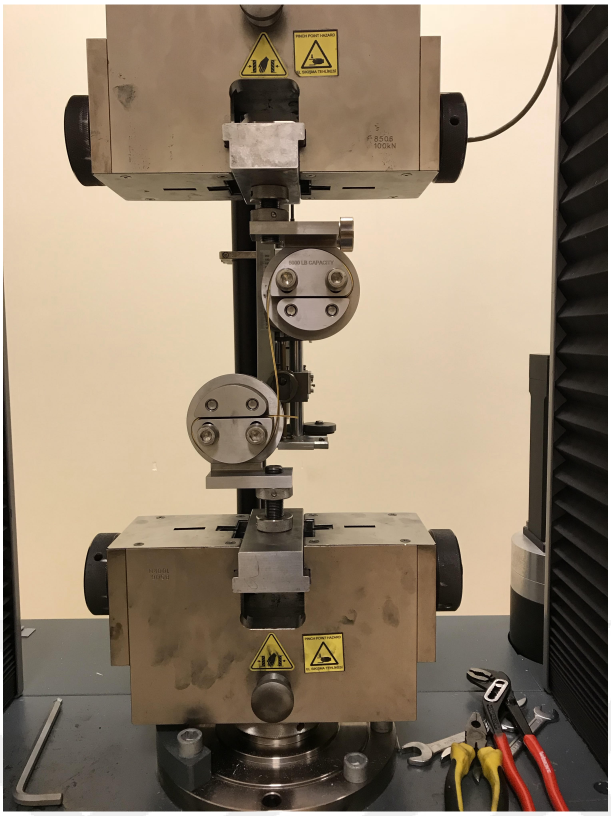

**Figure 2.12** : Tensile testing of CNTs/PEI FDM filaments.

### 2.3.4 Four point probe volume conductivity measurements

Four point probe works with a current $I$ inputted by outer two contacts as seen in Figure 2.13 and inner two probe voltage drop $V$ is measured by inner contacts. The ratio of $V/I$ equals to sample resistance $R$. By using $R$, the resistivity $\rho$ can be calculated. Since we measured 3D samples which its thickness is higher than 1 mm, we have used these formulations to calculate resistivity [56].

The volume conductivity of reference PEI and CNTs/PEI filaments was measured by a Four-Point Probe measuring system FPP 470 (Entek Electronics, Turkey) at room temperature as seen in Figure 2.14. The dimensions of each specimen were around 2.5 cm length and 1 mm thickness. Prior to testing, the volume of specimens were polished to reduce surface roughness. Micolli [57] *et al.* reported the formulations to calculate conductivity by four point probe method:

$$R = \rho L/A \tag{2.2}$$

$$\rho = F \cdot V/A \tag{2.3}$$

where

$$F = F_1 \cdot F_2 \tag{2.4}$$

$$F_1 = ln2/ln[sinh(t/s)]/[sinh(t/2s)] \tag{2.5}$$

$$F_2 = [1 + s/(2l + s) - s/(2l + 2s) - 1/(2l + 4s) + 1/(2l + 5s)] \tag{2.6}$$

where $F_1$ is geometric correlation factor of finite thickness of sample and $F_2$ is the probe alignment in sample edge which were calculated as 0.89 and 0.84 respectively, and $R$ is sample resistance which equals to $V/I$ ratio. Also, $l$ is the distance of current probe, $s$ is specimen thickness, which were determined as 1 mm and 1 mm, respectively.

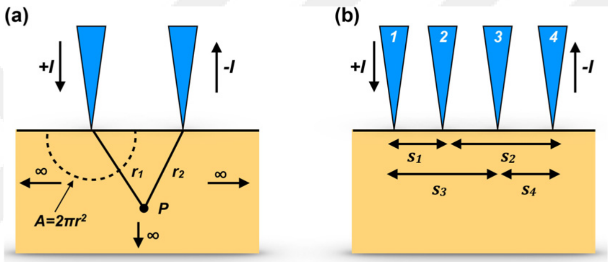


**Figure 2.13** : Four point probe array with contact spacing [56].


**Figure 2.14** : Four point probe conductivity measurement tool.

# 3. RESULTS AND DISCUSSION

## 3.1 Thermal Analysis of PEI and CNTs/PEI filaments

### 3.1.1 Thermal transition analysis on PEI and CNTs/PEI filaments

The DSC thermal analysis (Figure 3.1) revealed that the addition of CNTs didn't cause any changes in thermal transition compared to bulk polymer. Even though at high weight fraction of CNTs, $Tg$ of CNTs/PEI nanocomposites did not change and was similar to neat PEI. Measured $Tgs$ are 217, 215 and 216 °C for neat PEI, 5 wt % and 7wt % CNTs/PEI nanocomposite filaments, respectively.

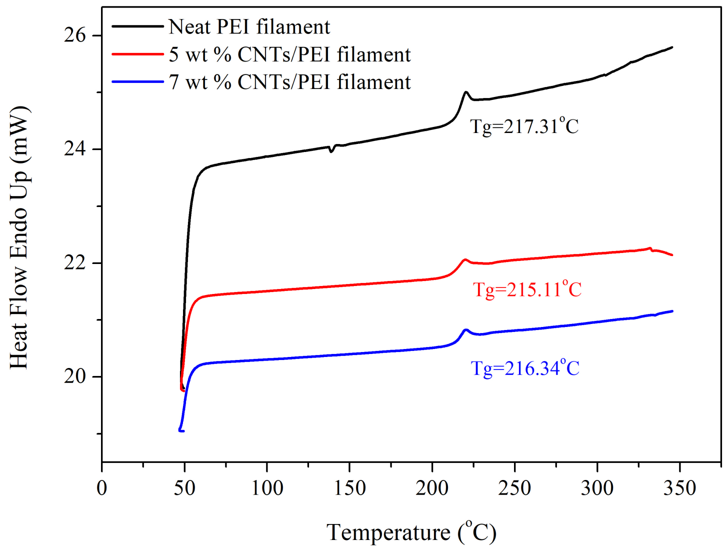


**Figure 3.1** : DSC curves of neat PEI and CNTs/PEI nanocomposite filaments.

Presence of CNTs in polymer matrix might not lead to significant deviations in thermal transition of polymer matrix nanocomposites [43, 58]. In this case, this pointed the interfacial adhesion between CNTs and PEI, that did not change mobility of polymer chains. For 3D printing applications, as experimental point of view, this meant to use same processing condition and print nanocomposite structures as smooth as original polymer was expected [14]. Pitchan *et al.* [39] observed that plasma and chemical functionalized CNTs addition into PEI let to shift in $Tg$ due to increase in CNTs fraction and hindered polymer chain mobility. This situation was related to increase in interfacial adhesion and enhanced wettability, that increased by CNTs fraction with restricted polymer chain movement. However, all these changes in polymer dynamics made the process conditions more challenging to handle such as increased process temperature, hence came up with poor resolution in printability. Besides, untreated CNTs incorporated composites didn't cause radical changes in $Tg$ [43, 44, 58, 59].

Hysteresis peak or enthalpic relaxation at $Tg$ has been widely seen in amorphous or semicrystallines polymers with low crystallinity [59]. Hysteresis peak was visible in neat PEI as seen in Figure 3.1. The hysteresis peak usually diminished by increase in crystallinity. The disappearance of hysteresis peak at both 5 and 7 wt % CNTs/PEI nanocomposites, which indicated increased crystallinity degree of PEI chains compared to neat polymer [59].

No significant change in $Tg$ with CNTs incorporation might be due to shortening of CNTs length [60] and their lack of effectiveness in reinforcing. Insignificant variation in $Tg$ also indicated poor wettability of CNTs with PEI. This result also supports observed relatively low improvement in tensile performance of filaments. But, poor wettability also contributed conductivity percolation with increasing possibility of CNTs interconnection pathway.

### 3.1.2 Thermal degradation analysis on PEI and CNTs/PEI filaments

Figure 3.2 reveals the thermal degradation properties of pellets fabricated by solution mixing of CNTs/PEI in NMP under nitrogen atmosphere. As it can be seen at around 200°C, there was a 10 wt % loss, at around boiling point of NMP. Hence, this caused rough nanocomposite filaments composed of CNTs/PEI pellets in processing and excess gas outlet. In addition to this observation, Figure 3.2 also suggests that NMP entrapped in CNTs/PEI pellets were not entirely removed during drying in a vacuum oven. Hence, this gas outlet, which was highlighted in Figure 3.3, observed during extrusion where rough filament surface was ended up.

Furthermore, filament diameters were much thicker than of 1.70 mm as revealed in Figure 3.3. Due to these process challenges and poor filament quality, the fabrication technique of nanocomposite filaments was changed.

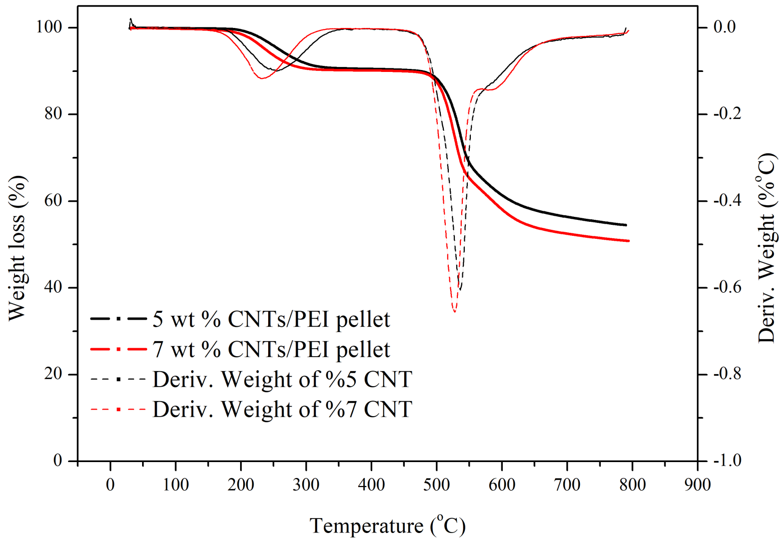


**Figure 3.2** : TGA curves of CNTs/PEI nanocomposite pellets under nitrogen atmosphere.

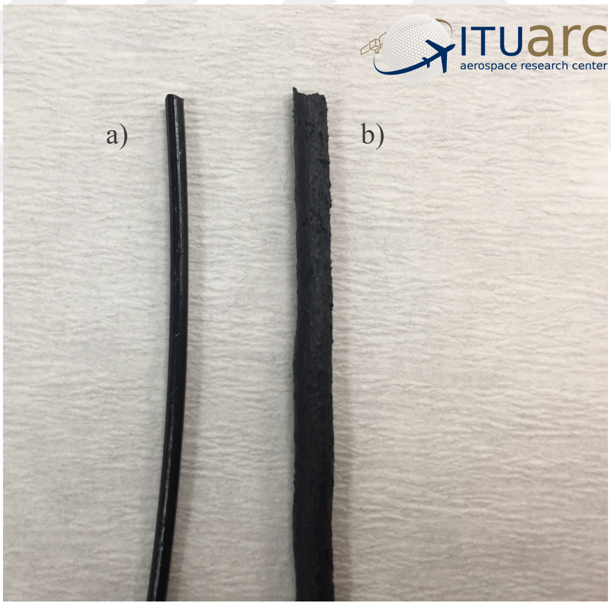


**Figure 3.3** : 5 wt % CNTs/PEI filaments fabricated by a) solely extrusion and b) after extrusion solvent mixing of CNTs and PEI in NMP.

Thermal stability of neat PEI and CNTs/PEI nanocomposite filaments was analyzed by TGA under air atmosphere as demonstrated in Figure 3.4. There were two primarily degradation peaks detected at around 550°C and 680°C. This result indicated molecular chain scission and residual species oxidation, respectively [43, 58, 61]. Furthermore, CNTs incorporation into PEI filament led to a slight shift in decomposition temperature $(Td)$ compared to neat PEI granule, where Td decreased by CNTs incorporation. Similar behavior was also observed by Pitchan *et al.* [39] in their functionalized CNTs reinforced PEI study.

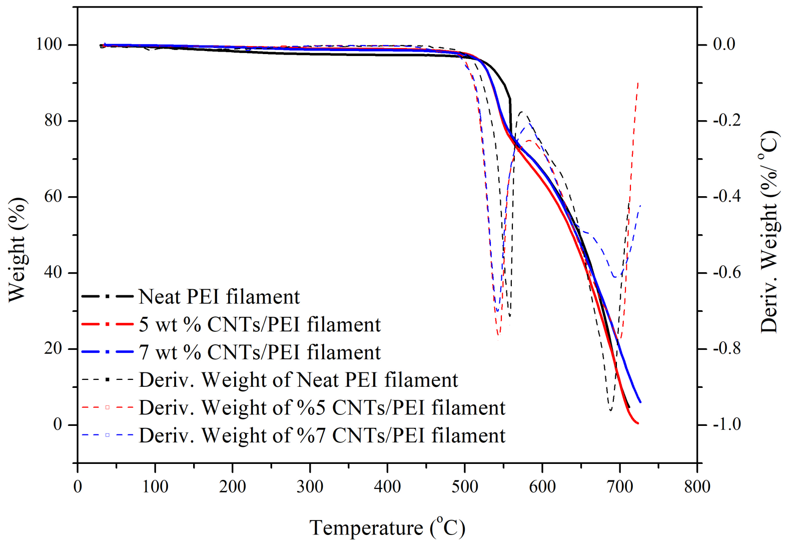


**Figure 3.4** : TGA curves of neat PEI and CNTs/PEI nanocomposite filaments under air atmosphere.

TGA characterization provides information for use in kinetic analysis and prediction of polymers lifetime in real atmosphere. Pitchan *et al.* [39] reported that incorporation of CNTs into PEI matrix led to increase activation energy for thermal degredation of polymer due to their dispersion. Higher value of activation energy compared to reference PEI indicated relatively enhanced thermal stability of CNTs/PEI nanocomposites. Thus, increase in activation energy of polymers pointed out higher thermal stability.

## 3.2 Morphological Analysis

### 3.2.1 Surface analysis on PEI and CNTs/PEI filaments

Figure 3.5 illustrates SEM micrographs of CNTs/PEI filaments at 5 and 7 wt % CNTs at different magnifications. Fracture surface analysis pointed the lack of nonwetted areas between CNTs and PEI matrix, which strongly was attributed to interface interaction. On the surface, CNTs were distributed homogeneously. This indicated that the benefits of melt-state mixing, following first twin-screw extrusion and further single-screw extrusion, without using any solvent or additives was an efficient technique to disperse CNTs in PEI matrix. Furthermore, Figure 3.5 (e,f) reveals that CNTs were effectively adhered to PEI matrix. The fibrillation of nanocomposites, which can be demonstrated in Figure 3.5 (e,f), was also observed by several researchers [37–39, 43, 59]. These brighter white lines and dots could be identified as the tail end of CNTs caused by cryogenic fracture. On the other hand, Isayev *et al.* [38] reported that untreated CNTs dispersion in PEI matrix could show entangled CNTs bundles with the size of 1 $\mu$m, which was attributed to inefficient shear stress applied during extrusion process. Hence, the lack of CNTs bundles on fracture surface emphasized the accuracy of shear rate of 100 rpm which eased to overcome CNTs aggregation problem in this study.

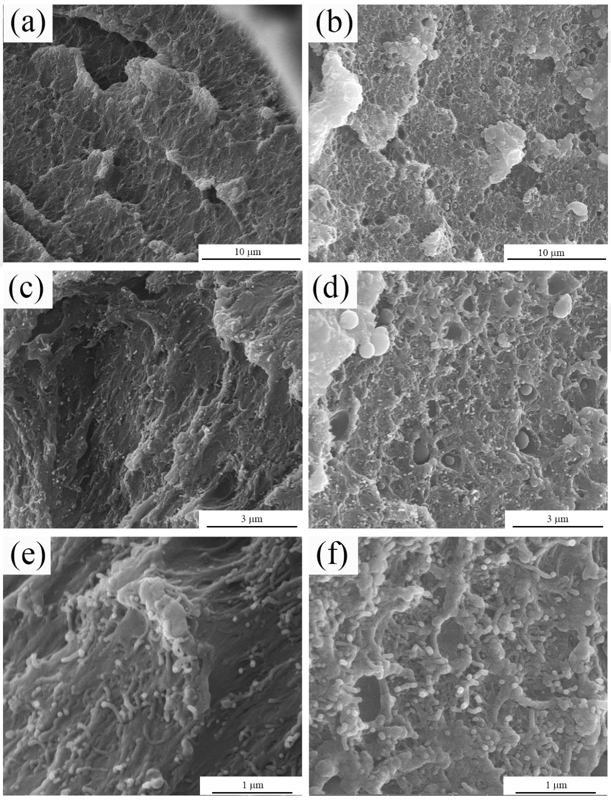


**Figure 3.5** : SEM images of 5 wt % (Left) and 7 wt % (Right) CNTs/PEI filaments at various magnifications (a,b) x10kX, (c,d) x30kX and (e,f) x80kX. CNTs can be identified as brighter points in the images.

### 3.2.2 Microstructure analysis

Figure 3.6 shows the TEM images of 7 wt % CNTs/PEI filaments at 30kX and 80kX magnifications. At higher CNTs concentration of 7 wt % CNTs/PEI images, homogeneous dispersion and distribution of CNTs were observed without any detectable nanotube reaggregation. In previous studies on exploring CNTs dispersion into high performance matrices [36, 37, 39, 44, 62], untreated CNTs were detected also as in the form of entangled CNTs bundles. This indicates that using both twin and single-screw extruders consecutively were effective in dispersing CNTs uniformly in PEI matrix. Furthermore, it is also reported that PEI was a good host for CNTs for composite applications [39]. It should be also noted CNTs were not only homogeneously dispersed and distributed but also oriented along extrusion direction, attributed to elongation flow through screw extruders and hindered mobility of CNTs in high viscous PEI chains [36]. All these factors positively contributed to tensile strength of nanocomposite filaments and reduction in electrical percolation threshold [37].

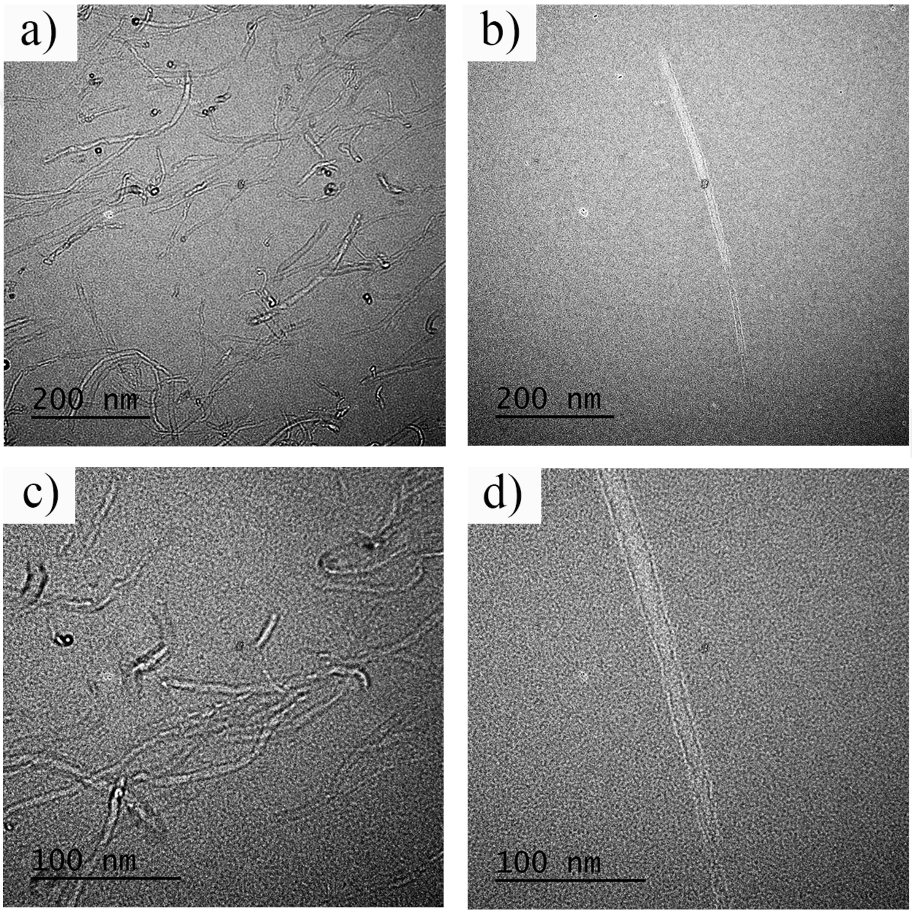


**Figure 3.6** : TEM micrographs of a,c) 7 and b,d) 0.1 wt % CNTs/PEI filaments with 30kX (above) and 80kX (below) magnification. The bright white lines were identified as CNTs in PEI matrix.

Mixing conditions considerably affect the dispersion state of polymer nanotube compositions. Rising melt mixing speed and mixing time led to higher specific mechanical energy while improving dispersion. Despite shorter residence time, increasing rotation speed in carbon nanotube polymer systems resulted in effective

CNTs dispersion [60]. Furthermore, size, area and number of CNTs agglomerates decreased with increasing mixing speed. The main drawback of applying high mixing speed was shortening of nanotubes. In the reference studies [63, 64], nanotubes were incorporated in PC by melt compounding and, after this process CNTs length were shortened from 1341 nm to 418 nm. Similarly, in this study CNTs length were decreased from around 1500 nm to around 305 nm due to twin screw extrusion which was repeated over five times at 100 rpm.

## 3.3 Quasi static tensile testing of PEI and CNTs/PEI filaments

Mechanical behavior of FDM filaments were summarized in Table 3.1 and representative graph averaged out 5 specimens was demonstrated in Figure 3.7. CNTs incorporation into PEI matrix led to increase in stiffness gradually. The changes in specific tensile modulus depended upon the interfacial shear strength, aspect ratio of nano-filler and its dispersion state and the degree of alignment of both nano-fillers and polymer chains [39]. The interfacial shear strength relies on the maximum stress transfer between polymer and CNTs, which was strongly affected by the nature of polymer-CNTs interface. Strong and well-bonded interface could be promoted by uniform dispersion of CNTs in polymer matrix. Thus, up to 10 wt % specific stiffness was reported by incorporation of CNT into PEI matrix. Increase in specific strength also emphasized on the efficient adhesiveness between polymer and nano-filler as well as homogeneous dispersion and orientation of CNTs in PEI matrix [39]. Specific strength of 5 wt % CNTs reinforced PEI filament was almost the same value with neat PEI filament. The reason would be the locally unevenness of nanocomposite filament due to manufacturing defects. As expected, the value of strain at break of non-reinforced PEI filament was much higher than all CNTs incorporated PEI filaments. This could be highlighted that CNTs addition led to increase in brittleness of filaments [43]. Furthermore, the density of filaments decreased relatively with the addition of CNTs. Although the addition of CNTs slightly enhanced mechanical performance of PEI filament, it was limited probably due to severe reduction in CNTs length during extrusion process. As a conclusion, CNTs incorporation into PEI resulted in increase in Young's modulus, tensile strength and also increase in brittleness of filaments.

**Table 3.1** : Quasi-static tensile properties of PEI and nanocomposite FDM filaments.

| Filament type | Specific stiffness ($kN.m/kg$) | Specific strength ($kN.m/kg$) | Elongation (%) | Density ($g/cm^3$) |
|---|---|---|---|---|
| Neat PEI filament | $800 \pm 31$ | $76 \pm 1.3$ | $49 \pm 3.34$ | 1.22 |
| 5 wt % CNTs/PEI filament | $854 \pm 40$ | $76 \pm 1.6$ | $12 \pm 0.53$ | 1.20 |
| 7 wt % CNTs/PEI filament | $951 \pm 13$ | $83 \pm 3.1$ | $14 \pm 1.65$ | 1.19 |

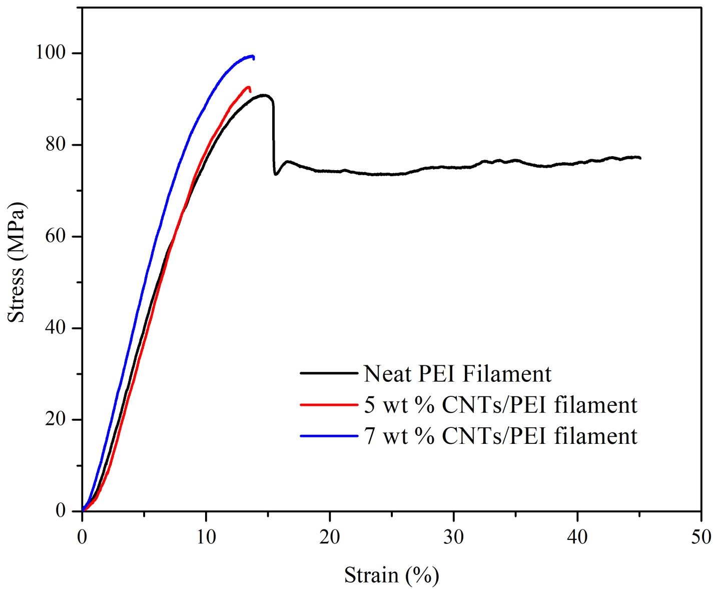


**Figure 3.7** : Representative stress-strain graph of neat PEI, 5 and 7 wt % CNTs/PEI filaments.

Specific strength of commodity thermoplastics such as PP, LDPE, HDPE, PS, and PA which were around 37, 64, 27, 44 and 53 kN.m/kg, respectively, reported by reference study in [65]. Compared to these polymers, high performance PEI exbitied much higher specific stiffness of 76 kN.m/kg. Similar values were detected among other high performance polymers such as PEEK with specific strength of around 78 kN.m/kg was reported by reference study [44]. For applications which demands high strength to weight ratio such as aerospace, high performance polymers have significant advantage particularly regarding to metals. For instance, compared to stainless steel with 60 kN.m/kg [66], the use of PEI would be a good alternative to replace metal and metal alloys used in advanced applications. Pitchan *et al.* [39] reported that by replacing metal usage with CNTs reinforced polymers in air-frames it is possible to save 9.8 % fuel by increasing flight range by 13.2 %.

## 3.4 Volume conductivity and electrical percolation network of CNTs/PEI filaments

Table 3.2 reveals the effect of CNTs incorporation in PEI matrix with respect to weight fractions. Similar to Dul *et al.*'s [43] observations, electrical conductivity increased as rise in CNTs content. Compared to neat sample, a tremendous improvement in electrical conductivity was detected in all CNTs/PEI compositions due to uniform distribution of CNTs into PEI matrix. In the study of Isayev *et al.* [38], volume conductivity of 10 wt % CNTs/PEI samples were noted as around $10^{-5}$ S/cm for all treated and untreated CNTs reinforced PEI nanocomposites.

Figure 3.8 demonstares the electrical percolation of CNTs/PEI filaments. Electrical percolation theory [67, 68] estimates the minimum amount of conductive nanofiller ($\phi_c$) to make composite conductive. In previous studies, $\phi_c$ was around 0.67 wt % for CNTs/PLA [69] nanocomposites and 0.49 wt % for CNTs/PBI [42] composites. Figure 3.8 suggested that electrical percolation threshold between 0.1 and 0.25 wt % CNTs/PEI. Compared to reference studies [42,69,70], percolation threshold estimated in this thesis was increasingly lower. Pötschke *et al.* [70] reported that low percolation threshold was result of high aspect ratio of nanofiller. However, the nanocomposites produced by applying twin screw extrusion process, which led to severe reduction in CNTs length reduced around 300 nm. This can be attributed that intense mixing by melt compounding led to homogeneous and uniform dispersion and distribution of CNTs to create interconnected pathway at low nanofiller fractions.

Rheological behavior of polymer structures could be assessed to identify electrical percolation threshold of composites. In the rheological point of view, CNTs addition resulted increase in complex viscosity specifically at low frequencies as observed in several researches [37, 70]. Pötschke *et al.* [70] investigated CNTs/PC rheological and electrical behavior compared to reference neat PC. Pure PC and CNTs/PC nanocomposites using lower than 2 wt % fractions showed Newtonian plateau with increasing frequency and exhibited $10^3$ Pa.s viscosity at low frequencies. On the other hand, high CNTs content filled PC (>2 wt %)showed significant and gradual increase

**Table 3.2** : Electrical conductivity of various CNTs fractions in PEI matrix.

| CNTs wt % in PEI matrix | Volume conductivity (S/cm) |
|---|---|
| 0 | $10^{-15}$ |
| 0.1 | $1.25 \times 10^{-5}$ |
| 0.25 | $1.67 \times 10^{-3}$ |
| 0.5 | $1.77 \times 10^{-3}$ |
| 2 | $4.23 \times 10^{-3}$ |
| 5 | $1.69 \times 10^{-1}$ |
| 7 | $2.57 \times 10^{-1}$ |

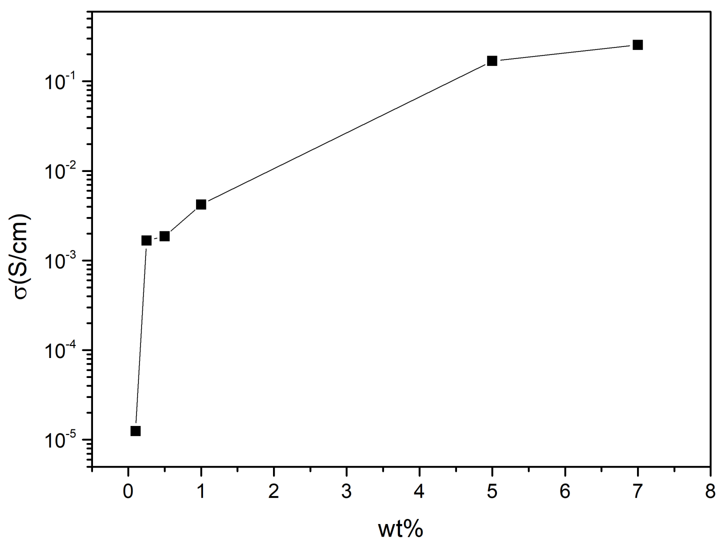


**Figure 3.8** : Estimation of percolation threshold in CNTs/PEI filaments at different CNTs content.

with CNTs addition in complex viscosity up to 4 order of magnitude for 15 wt % masterbatch. Also, electrical percolation threshold was also estimated between 1 and 2 wt % CNTs/PC similar to rheological percolation. Furthermore, strong shear thinning effect was observed in nanocomposites with high CNTs loading. Similarly, Lozano *et al.* [71] reported melt viscosity threshold of 10 wt % for nanofiber/PP composition corresponding to electrical percolation threshold at low frequencies. Composites containing less than 10 wt % nanofiber obeyed closely the viscosity-frequency characteristic of neat PP. Thus, it could be suggested that melt viscosity percolation of CNTs/PEI nanocomposites might be around 0.1 and 0.25 wt

%. CNTs/PEI composition with higher weight fractions than 0.25 wt % possibly have strong shear thinning behavior compared to neat PEI.

### 3.5 Preliminary results on 3D printing of CNTs/PEI pieces

As Figure 3.9 represents the 3D printed preliminary trials composed of 5 wt % CNTs/PEI and neat PEI filaments. In the future studies of this thesis cellular structures will be print out for use in high performance aerospace applications.

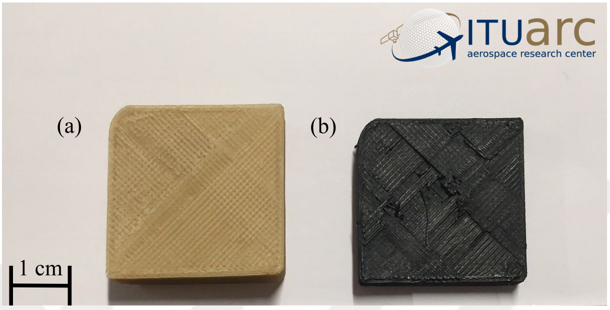


**Figure 3.9** : 3D printed preliminary samples composed of a) neat PEI and b) 5 wt % CNTs/PEI filaments.

# 4. CONCLUSION

In this thesis, neat PEI and CNTs/PEI filament at CNTs different fractions were fabricated for later use in 3D printing applications. The neat PEI filament was fabricated by using single-screw extruder without using any solvent or additives. The nanocomposite filaments were produced by combination of twin and single-screw extruders. To ensure homogeneous CNTs dispersion in PEI matrix to enhance the electrical conductivity and mechanical performance, twin-screw extrusion was processed for five times and then nanocomposite stands was granulized to be later fed into the extruder. Thereafter, CNTs reinforced nanocomposite filaments were fabricated by single screw extrusion with standard FDM filament of 1.70 *mm* for additive manufacturing. Neat and CNTs/PEI filaments were characterized by thermal analysis (DSC and TGA), morphological investigations (SEM and TEM), tensile testing and four point probe conductivity measurements. DSC analysis reported that introduction of CNTs did not change thermal transitions of PEI, whereas TGA analysis revealed that CNTs incorporation into PEI led to a slight shift in decomposition temperature. It was noted that CNTs addition didn't change kinetic properties of original PEI, which is an important knowledge to set process temperature in 3D printing applications. Morphological analysis of both SEM and TEM micrographs displayed CNTs were homogeneously dispersed and distributed in PEI matrix. Furthermore, TEM images clearly indicated that CNTs were also oriented in the same direction without exhibiting any curvy structures or individual CNTs. These properties contributed to tensile strength and enabling lower percolation threshold of CNTs/PEI filaments. Electrical conductivity measurements by four-point probe showed that CNTs incorporation into the PEI matrix significantly increased the conductivity of nanocomposite filaments. For 7 wt % CNTs/PEI filaments, volume conductivity was $2.57 \times 10^{-1}$ S/cm, where conductivity of neat PEI filament was at around $10^{-15}$ S/cm. It is also worth to note that this increase in CNTs fraction also increased electrical conductivity. Moreover, percolation threshold of the nanocomposite filament was estimated between 0.1 and 0.25 wt % CNTs/PEI, which was lower than compared to reference studies in literature. Tensile test results demonstrated the changes in tensile strength due to increased CNTs concentration of 7 wt %. Consequently, in this thesis, neat PEI and multifunctional CNTs/PEI filaments were successfully fabricated for later use in additive manufacturing. The results highlighted that consecutive use of both twin and single-screw extruders for filament fabrication was an efficient way to distribute CNTs into PEI filament. Furthermore, it was worth to note that PEI was good host to disperse CNTs without any requirement of solvent or additives. Moreover, these CNTs/PEI filaments have promising thermal, electrical and mechanical quality for their use in aerospace applications due to their high thermal and mechanical stability.

## REFERENCES


[1] **Campbell, T.A. and Ivanova, O.S.** (2013). 3D printing of multifunctional nanocomposites, *Nano Today*, *8*(2), 119–120.

[2] **Kim, M.S.**, **Chu, W.S.**, **Kim, Y.M.**, **Avila, A.P.G. and Ahn, S.H.** (2009). Direct metal printing of 3D electrical circuit using rapid prototyping, *International Journal of Precision Engineering and Manufacturing*, *10*(5), 147–150.

[3] **Eckel, Z.C.**, **Zhou, C.**, **Martin, J.H.**, **Jacobsen, A.J.**, **Carter, W.B. and Schaedler, T.A.** (2016). Additive manufacturing of polymer-derived ceramics, *Science*, *351*(6268), 58–62.

[4] **Tymrak, B.**, **Kreiger, M. and Pearce, J.M.** (2014). Mechanical properties of components fabricated with open-source 3-D printers under realistic environmental conditions, *Materials & Design*, *58*, 242–246.

[5] **Tran, P.**, **Ngo, T.D.**, **Ghazlan, A. and Hui, D.** (2017). Bimaterial 3D printing and numerical analysis of bio-inspired composite structures under in-plane and transverse loadings, *Composites Part B: Engineering*, *108*, 210–223.

[6] **Melnikova, R.**, **Ehrmann, A. and Finsterbusch, K.** (2014). 3D printing of textile-based structures by Fused Deposition Modelling (FDM) with different polymer materials, *IOP Conference Series: Materials Science and Engineering*, volume 62, IOP Publishing, p.012018.

[7] **Caulfield, B.**, **McHugh, P. and Lohfeld, S.** (2007). Dependence of mechanical properties of polyamide components on build parameters in the SLS process, *Journal of Materials Processing Technology*, *182*(1-3), 477–488.

[8] **Garcia, C.R.**, **Correa, J.**, **Espalin, D.**, **Barton, J.H.**, **Rumpf, R.C.**, **Wicker, R. and Gonzalez, V.** (2012). 3D printing of anisotropic metamaterials, *Progress In Electromagnetics Research*, *34*, 75–82.

[9] **Kroll, E. and Artzi, D.** (2011). Enhancing aerospace engineering students' learning with 3D printing wind-tunnel models, *Rapid Prototyping Journal*, *17*(5), 393–402.

[10] **Wong, K.V. and Hernandez, A.** (2012). A review of additive manufacturing, *ISRN Mechanical Engineering*, *2012*.

[11] **Short, D.B.** (2015). Use of 3D printing by museums: Educational exhibits, artifact education, and artifact restoration, *3D Printing and Additive Manufacturing*, *2*(4), 209–215.

[12] **Murphy, S.V. and Atala, A.** (2014). 3D bioprinting of tissues and organs, *Nature biotechnology*, *32*(8), 773.

[13] **Wang, X.**, **Jiang, M.**, **Zhou, Z.**, **Gou, J. and Hui, D.** (2017). 3D printing of polymer matrix composites: A review and prospective, *Composites Part B: Engineering*, *110*, 442–458.

[14] **Lee, J.Y.**, **An, J. and Chua, C.K.** (2017). Fundamentals and applications of 3D printing for novel materials, *Applied Materials Today*, *7*, 120–133.

[15] **de Leon, A.C.**, **Chen, Q.**, **Palaganas, N.B.**, **Palaganas, J.O.**, **Manapat, J. and Advincula, R.C.** (2016). High performance polymer nanocomposites for additive manufacturing applications, *Reactive and Functional Polymers*, *103*, 141–155.

[16] **Martin, J.H.**, **Yahata, B.D.**, **Hundley, J.M.**, **Mayer, J.A.**, **Schaedler, T.A. and Pollock, T.M.** (2017). 3D printing of high-strength aluminium alloys, *Nature*, *549*(7672), 365.

[17] **Appleyard, D.** (2015). Powering up on powder technology, *Metal Powder Report*, *70*(6), 285–289.

[18] **Watkins, T.**, **Bilheux, H.**, **An, K.**, **Payzant, A.**, **Dehoff, R.**, **Duty, C.**, **Peter, W.**, **Blue, C. and Brice, C.A.** (2013). Neutron characterization for additive manufacturing.

[19] **Invernizzi, M.**, **Natale, G.**, **Levi, M.**, **Turri, S. and Griffini, G.** (2016). UV-assisted 3D printing of glass and carbon fiber-reinforced dual-cure polymer composites, *Materials*, *9*(7), 583.

[20] **Misra, A.K.**, **Grady, J.E. and Carter, R.** (2015). Additive Manufacturing of Aerospace Propulsion Components.

[21] **Url-5** (2018). 3D Printed Composites – Faster, Stronger, More Materials, *http://impossibleobjects.com*.

[22] **Biron, M.** (2012). *Thermoplastics and thermoplastic composites*, William Andrew.

[23] **Mittal, K.L.** (2013). *Polyimides: synthesis, characterization, and applications*, volume 1, Springer Science & Business Media.

[24] **academy, P.** (2017). Polyetherimide (PEI), *Polymer academy. https://polymeracademy.com/polyetherimide/*.

[25] **Giles Jr, H.F.**, **Mount III, E.M. and Wagner Jr, J.R.** (2004). *Extrusion: the definitive processing guide and handbook*, William Andrew.

[26] **Pethrick, R.A.** (2010). *Polymer science and technology for scientists and engineers*, Whittles Publishing.

[27] **Loos, M.** (2014). *Carbon nanotube reinforced composites: CNT Polymer Science and Technology*, Elsevier.

[28] **Iijima, S.** (1991). Helical microtubules of graphitic carbon, *nature*, *354*(6348), 56.

[29] **Baughman, R.H.**, **Zakhidov, A.A. and De Heer, W.A.** (2002). Carbon nanotubes–the route toward applications, *science*, *297*(5582), 787–792.

[30] **Kim, Y.J.**, **Shin, T.S.**, **Do Choi, H.**, **Kwon, J.H.**, **Chung, Y.C. and Yoon, H.G.** (2005). Electrical conductivity of chemically modified multiwalled carbon nanotube/epoxy composites, *Carbon*, *43*(1), 23–30.

[31] **Dresselhaus, M.**, **Lin, Y.**, **Rabin, O.**, **Jorio, A.**, **Souza Filho, A.**, **Pimenta, M.**, **Saito, R.**, **Samsonidze, G. and Dresselhaus, G.** (2003). Nanowires and nanotubes, *Materials Science and Engineering: C*, *23*(1-2), 129–140.

[32] **Binns, C.** (2010). *Introduction to nanoscience and nanotechnology*, volume 14, John Wiley & Sons.

[33] **Qin, Z.**, **Qin, Q.H. and Feng, X.Q.** (2008). Mechanical property of carbon nanotubes with intramolecular junctions: Molecular dynamics simulations, *Physics Letters A*, *372*(44), 6661–6666.

[34] **Collins, P.G.**, **Arnold, M.S. and Avouris, P.** (2001). Engineering carbon nanotubes and nanotube circuits using electrical breakdown, *science*, *292*(5517), 706–709.

[35] **Spitalsky, Z.**, **Tasis, D.**, **Papagelis, K. and Galiotis, C.** (2010). Carbon nanotube–polymer composites: chemistry, processing, mechanical and electrical properties, *Progress in polymer science*, *35*(3), 357–401.

[36] **Socher, R.**, **Krause, B.**, **Müller, M.T.**, **Boldt, R. and Pötschke, P.** (2012). The influence of matrix viscosity on MWCNT dispersion and electrical properties in different thermoplastic nanocomposites, *Polymer*, *53*(2), 495–504.

[37] **Bangarusampath, D.**, **Ruckdäschel, H.**, **Altstädt, V.**, **Sandler, J.K.**, **Garray, D. and Shaffer, M.S.** (2009). Rheology and properties of melt-processed poly (ether ether ketone)/multi-wall carbon nanotube composites, *Polymer*, *50*(24), 5803–5811.

[38] **Isayev, A.**, **Kumar, R. and Lewis, T.M.** (2009). Ultrasound assisted twin screw extrusion of polymer–nanocomposites containing carbon nanotubes, *Polymer*, *50*(1), 250–260.

[39] **Pitchan, M.K.**, **Bhowmik, S.**, **Balachandran, M. and Abraham, M.** (2016). Effect of surface functionalization on mechanical properties and decomposition kinetics of high performance polyetherimide/MWCNT nano composites, *Composites Part A: Applied Science and Manufacturing*, *90*, 147–160.

[40] **Ghoshal, S.** (2017). Polymer/carbon nanotubes (CNT) nanocomposites processing using additive manufacturing (three-dimensional printing) technique: An overview, *Fibers*, *5*(4), 40.

[41] **Zhang, D.**, **Chi, B.**, **Li, B.**, **Gao, Z.**, **Du, Y.**, **Guo, J. and Wei, J.** (2016). Fabrication of highly conductive graphene flexible circuits by 3D printing, *Synthetic Metals*, *217*, 79–86.

[42] **Gnanasekaran, K.**, **Heijmans, T.**, **van Bennekom, S.**, **Woldhuis, H.**, **Wijnia, S.**, **Friedrich, H.** *et al.* (2017). 3D printing of CNT-and graphene-based conductive polymer nanocomposites by fused deposition modeling, *Applied Materials Today*, *9*, 21–28.

[43] **Dul, S.**, **Fambri, L. and Pegoretti, A.** (2018). Filaments Production and Fused Deposition Modelling of ABS/Carbon Nanotubes Composites, *Nanomaterials*, *8*(1), 49.

[44] **Berretta, S.**, **Davies, R.**, **Shyng, Y.**, **Wang, Y. and Ghita, O.** (2017). Fused Deposition Modelling of high temperature polymers: Exploring CNT PEEK composites, *Polymer Testing*, *63*, 251–262.

[45] **NMP** (2017). NMP, *https://productcatalog.eastman.com/tds/ProdDatasheet.aspx?product=71103627*.

[46] **DMAc** (2017). DMAc, *http://aventelfrance.com/product/download/27*.

[47] **Zhang, X.**, **Yin, Q.**, **Li, X.**, **Zhang, M.**, **Huang, J.**, **Wang, C.**, **Zhang, Z.**, **Huang, Y.**, **Guo, M. and Li, Y.** (2017). Solubility and mixing thermodynamics properties of erythromycin ethylsuccinate in different organic solvents, *Journal of Molecular Liquids*, *237*, 46–53.

[48] **Kim, K.**, **Park, J.**, **Suh, J.h.**, **Kim, M.**, **Jeong, Y. and Park, I.** (2017). 3D printing of multiaxial force sensors using carbon nanotube (CNT)/thermoplastic polyurethane (TPU) filaments, *Sensors and Actuators A: Physical*, *263*, 493–500.

[49] **Url-2** (2014). DSC Beginners Guide, *https://www.perkinelmer.com/CMSResources/Images/4474542GDE_DSCBeginnersGuide.pdf*.

[50] **Url-3** (2011). Importance of DSC Rapid Cooling for the Analysis of Plastic Microwave Food Trays, *https://www.perkinelmer.com/labsolutions/resources/docs/APP_010009_01_APP_Importance_of_DSC_Rapid_Cooling_fo_%20the_Analysis_of_Plastic_Microwave_Food_Trays.pdf*.

[51] **Url-4** (2011). Characterization of Polymers Using TGA, *http://depts.washington.edu/mseuser/Equipment/RefNotes/TGA_Notes.pdf*.

[52] **Singh, A.K.** (2015). *Engineered nanoparticles: structure, properties and mechanisms of toxicity*, Academic Press.

[53] **Williams, D.B. and Carter, C.B.**, (1996). The transmission electron microscope, Transmission electron microscopy, Springer, pp.3–17.

[54] **Walker, J.**, **Reiner, J. and Solenthaler, C.** (1995). Focused ion beam sample preparation for TEM, *MICROSCOPY OF SEMICONDUCTING MATERIALS 1995*, *146*, 629–634.

[55] **Jublot, M. and Texier, M.** (2014). Sample preparation by focused ion beam micromachining for transmission electron microscopy imaging in front-view, *Micron*, *56*, 63–67.

[56] **Miccoli, I.**, **Edler, F.**, **Pfnür, H. and Tegenkamp, C.** (2015). The 100th anniversary of the four-point probe technique: the role of probe geometries in isotropic and anisotropic systems, *Journal of Physics: Condensed Matter*, *27*(22), 223201.

[57] **Miccoli, I.**, **Edler, F.**, **Pfnür, H. and Tegenkamp, C.** (2015). The 100th anniversary of the four-point probe technique: the role of probe geometries in isotropic and anisotropic systems, *Journal of Physics: Condensed Matter*, *27*(22), 223201.

[58] **Yang, S.**, **Castilleja, J.R.**, **Barrera, E. and Lozano, K.** (2004). Thermal analysis of an acrylonitrile–butadiene–styrene/SWNT composite, *Polymer Degradation and Stability*, *83*(3), 383–388.

[59] **Hegde, M.**, **Samulski, E.T.**, **Rubinstein, M. and Dingemans, T.J.** (2015). The role of crystallinity in SWCNT–polyetherimide nanocomposites, *Composites Science and Technology*, *110*, 176–187.

[60] **Pötschke, P.**, **Villmow, T. and Krause, B.** (2013). Melt mixed PCL/MWCNT composites prepared at different rotation speeds: Characterization of rheological, thermal, and electrical properties, molecular weight, MWCNT macrodispersion, and MWCNT length distribution, *Polymer*, *54*(12), 3071–3078.

[61] **Hong, N.**, **Zhan, J.**, **Wang, X.**, **Stec, A.A.**, **Hull, T.R.**, **Ge, H.**, **Xing, W.**, **Song, L. and Hu, Y.** (2014). Enhanced mechanical, thermal and flame retardant properties by combining graphene nanosheets and metal hydroxide nanorods for Acrylonitrile–Butadiene–Styrene copolymer composite, *Composites Part A: Applied Science and Manufacturing*, *64*, 203–210.

[62] **Pitchan, M.K.**, **Bhowmik, S.**, **Balachandran, M. and Abraham, M.** (2017). Process optimization of functionalized MWCNT/polyetherimide nanocomposites for aerospace application, *Materials & Design*, *127*, 193–203.

[63] **Krause, B.**, **Boldt, R. and Pötschke, P.** (2011). A method for determination of length distributions of multiwalled carbon nanotubes before and after melt processing, *Carbon*, *49*(4), 1243–1247.

[64] **Krause, B.**, **Villmow, T.**, **Boldt, R.**, **Mende, M.**, **Petzold, G. and Pötschke, P.** (2011). Influence of dry grinding in a ball mill on the length of multiwalled carbon nanotubes and their dispersion and percolation behaviour in melt mixed polycarbonate composites, *Composites Science and Technology*, *71*(8), 1145–1153.

[65] **Ku, H.**, **Wang, H.**, **Pattarachaiyakoop, N. and Trada, M.** (2011). A review on the tensile properties of natural fiber reinforced polymer composites, *Composites Part B: Engineering*, *42*(4), 856–873.

[66] **Url-6** (2018). Stainless Steel, *http://temperedmetals.com/stainless-steel-type-3163 16l/.*

[67] **Pike, G. and Seager, C.** (1974). Percolation and conductivity: A computer study. I, *Physical review B*, *10*(4), 1421.

[68] **Seager, C. and Pike, G.** (1974). Percolation and conductivity: A computer study. II, *Physical Review B*, *10*(4), 1435.

[69] **Postiglione, G.**, **Natale, G.**, **Griffini, G.**, **Levi, M. and Turri, S.** (2015). Conductive 3D microstructures by direct 3D printing of polymer/carbon nanotube nanocomposites via liquid deposition modeling, *Composites Part A: Applied Science and Manufacturing*, *76*, 110–114.

[70] **Pötschke, P.**, **Fornes, T. and Paul, D.** (2002). Rheological behavior of multiwalled carbon nanotube/polycarbonate composites, *Polymer*, *43*(11), 3247–3255.

[71] **Lozano, K. and Barrera, E.** (2001). Nanofiber-reinforced thermoplastic composites. I. Thermoanalytical and mechanical analyses, *Journal of Applied Polymer Science*, *79*(1), 125–133.

**CURRICULUM VITAE**

**Name Surname:** Özge KAYNAN

**Place and Date of Birth:** Istanbul, 25/01/1992

**E-Mail:** ozgekaynan@gmail.com

**EDUCATION:**

- **B.Sc.:** 2016, Istanbul Technical University, Faculty of Textile Technologies and Design, Textile Engineering
- **M.Sc.:** 2018, Istanbul Technical University, Faculty of Textile Technologies and Design, Textile Engineering

**Journal Papers**

- Kaynan, O., Atescan, Y, Ozden-Yenigun, E., Cebeci, H. (2018). Mixed Mode Delamination in Carbon Nanotube Nanofiber Interlayered Composites. *Composites Part B*. (Accepted for publication)
- Sayilan, A., Kaynan, O., Yusifova, A, Cebeci, H., Ozden Yenigun, E. (2017). Design and Development of 3D Printed High Performance Textile Structures for Composites. *Journal of Textiles and Engineer, 24*(105). doi: 10.7216/1300759920172410502
- Tas, S., Kaynan, O., Ozden Yenigun, E., Nijmeijer, K. (2016). Polyacrylonitrile (PAN)/crown ether composite nanofibers for the selective adsorption of cations. *RSC Advances, 6*(5). doi: 10.1039/C5RA23214G

**Conference Publications**

- Kaynan, O., Yildiz, A., Cebeci, H., Ozden-Yenigun, E. (2018). CNTs Incorporated High Performance Electrically Conductive Thermoplastic Filaments for Additive Manufacturing. In *AUTEX 2018 World Textile Conference*. (Oral presentation)
- Kaynan, O., Atescan, Y., Jahangiri, S., Cebeci, H., Ozden-Yenigun, E. (2017). The Effects of Interlayered Carbon Nanotube Reinforced Electrospun Nanofibers on Mixed Mode Fracture Characteristics. In *21th International Conference on Composite Materials (ICCM-21)*. (Oral presentation)
- Kaynan, O., Jahangiri, S., Aravi, I., Işıkel ¸ Sanlı, J., Menceloğlu , Y., Ozden-Yenigun, E., Coaxial Electrospinning of PBI/SPEEK core/sheath nanofibers, *VI. National Polymer Science and Technology Conference*, 4-7 September, 2016, Ankara, Turkey (Oral presentation)